JAERI - M
92-020

INDC (JPN)-154/L

MEASUREMENT OF FORMATION CROSS SECTIONS OF SHORT-LIVED NUCLEI BY 14 MeV NEUTRONS

— F, Mg, Si, Ti, Cr, Ni, Ga, Rb, Sr, Ag —

March 1992

Kiyoshi KAWADE*, Hiroshi YAMAMOTO*, Takashi KOBAYASHI*
Toshio KATOH*, Toshiyuki IIDA** and Akito TAKAHASHI**

日 本 原 子 力 研 究 所
Japan Atomic Energy Research Institute

JAERI-Mレポートは，日本原子力研究所が不定期に公刊している研究報告書です。
入手の問合わせは，日本原子力研究所技術情報部情報資料課（〒319-11茨城県那珂郡東海村）あて，お申しこしください。なお，このほかに財団法人原子力弘済会資料センター（〒319-11 茨城県那珂郡東海村日本原子力研究所内）で複写による実費頒布をおこなっております。

JAERI-M reports are issued irregularly.
Inquiries about availability of the reports should be addressed to Information Division Department of Technical Information, Japan Atomic Energy Research Institute, Tokai-mura, Naka-gun, Ibaraki-ken 319-11, Japan.

編集兼発行　日本原子力研究所
印　　刷　いばらき印刷㈱

JAERI-M 92-020

Measurement of Formation Cross Sections of Short-lived Nuclei by 14 MeV Neutrons
- F, Mg, Si, Ti, Cr, Ni, Ga, Rb, Sr, Ag -

Kiyoshi KAWADE*, Hiroshi YAMAMOTO*, Takashi KOBAYASHI*
Toshio KATOH*, Toshiyuki IIDA** and Akito TAKAHASHI**

Department of Physics
Tokai Research Establishment
Japan Atomic Energy Research Institute
Tokai-mura, Naka-gun, Ibaraki-ken

(Received January 29, 1992)

Sixteen neutron activation cross sections for (n,2n), (n,p), (n,n'p) and (n,α) reactions producing short-lived nuclei with half-lives between 20 s and 7 min have been measured in the energy range of 13.4 to 14.9 MeV for F, Mg, Si, Ti, Cr, Ni, Ga, Rb, Sr and Ag.

Seven half-lives of short-lived nuclei produced by 14 MeV or thermal neutron bombardments were measured with Ge detectors for ^{51}Ti, ^{60m}Co, ^{88}Rb, ^{91g}Mo, ^{94}Y, ^{108}Ag and ^{109m}Pd in the spectrum multi-scaling mode.

Keywords: Activation, Cross Section, 14 MeV Neutron, Short-lived Nucleus, Half-life, Measurement, Ge Detector

---

This work was performed under the contract between Japan Atomic Energy Research Institute and Nagoya University.

* Nagoya University

** Osaka University

14MeV 中性子による短寿命核生成断面積の測定
－F, Mg, Si, Ti, Cr, Ni, Ga, Rb, Sr, Ag－

日本原子力研究所東海研究所物理部
河出　清*・山本　洋*・小林　隆*・加藤　敏郎*
飯田　敏行**・高橋　亮人**

（1992年1月29日受理）

半減期が20秒から7分程度の短寿命核生成断面積の測定を，中性子エネルギー13.4から14.9 MeVの範囲にわたり，F, Mg, Si, Ti, Cr, Ni, Ga, Rb, Sr, Agに対し (n,2n), (n,p), (n,n'p), (n,α) 反応，16断面積を測定した。

14 MeVまたは熱中性子照射で生成される短寿命核の半減期の測定を，^{51}Ti, ^{60m}Co, ^{88}Rb, ^{91g}Mo, ^{94}Y, ^{108}Ag, ^{109m}Pdの7核種について，Ge検出器を用いてスペクトルマルチスケーリングモードで行なった。

本報告書は，日本原子力研究所が名古屋大学に委託して行なった研究の成果である。
東海研究所：〒319－11　茨城県那珂郡東海村白方字白根2－4
*　名古屋大学
**　大阪大学

Contents

目　　次

1. Introduction

Neutron cross section data around 14 MeV are compiled as the evaluated data for fusion reactor technology, especially for calculations on radiation damage, nuclear transmutation, induced activity and so on. A lot of experimental data have been reported, but formation cross sections of short-lived nuclei have often not been measured in a reasonable accuracy and there are no available data for some reactions, because of difficulty in measuring short-lived nuclei. Moreover, there are often inconsistencies among the existing experimental data. We started systematic measurements of formation cross sections of short-lived nuclei 4 years ago. Up to now, 31 reactions were measured[1,2]. In the present work, 16 cross sections for the (n,2n), (n,p), (n,n'p) and (n,α) reactions leading to short-lived nuclei with half-lives between 20 s and 7 min were measured in the energy range of 13.4 to 14.9 MeV by the activation method.

The half-life is one of the most fundamental constants of the radioactive isotopes. In the activation cross section measurements, the uncertainty of the half-life brings a strong effect on the results. Seven half-lives of short-lived nuclei were measured with Ge detectors in a spectrum multi-scaling mode. Measured reactions and half-lives are shown in Table 1 and Table 2, respectively.

2. Measurement of Activation Cross Sections

The activation cross section values are obtained by measuring the radioactivities induced with neutron irradiations as follows:

$$C = N \sigma \phi \varepsilon I\gamma (1 - e^{-\lambda t_i}) e^{-\lambda t_c} (1 - e^{-\lambda t_m})/\lambda,$$

where

C : γ-ray peak counts,
N : atomic number of target nuclide,
σ : activation cross section measured,
φ : neutron flux at the irradiation position,
ε : detection efficiency of γ-ray peak,
Iγ : γ-ray emission probability per disintegration,

1. Introduction

Neutron cross section data around 14 MeV are compiled as the evaluated data for fusion reactor technology, especially for calculations on radiation damage, nuclear transmutation, induced activity and so on. A lot of experimental data have been reported, but formation cross sections of short-lived nuclei have often not been measured in a reasonable accuracy and there are no available data for some reactions, because of difficulty in measuring short-lived nuclei. Moreover, there are often inconsistencies among the existing experimental data. We started systematic measurements of formation cross sections of short-lived nuclei 4 years ago. Up to now, 31 reactions were measured[1,2]. In the present work, 16 cross sections for the (n,2n), (n,p), (n,n'p) and (n,α) reactions leading to short-lived nuclei with half-lives between 20 s and 7 min were measured in the energy range of 13.4 to 14.9 MeV by the activation method.

The half-life is one of the most fundamental constants of the radioactive isotopes. In the activation cross section measurements, the uncertainty of the half-life brings a strong effect on the results. Seven half-lives of short-lived nuclei were measured with Ge detectors in a spectrum multi-scaling mode. Measured reactions and half-lives are shown in Table 1 and Table 2, respectively.

2. Measurement of Activation Cross Sections

The activation cross section values are obtained by measuring the radioactivities induced with neutron irradiations as follows:

$$C = N \sigma \phi \varepsilon I\gamma (1 - e^{-\lambda t_i}) e^{-\lambda t_c} (1 - e^{-\lambda t_m})/\lambda,$$

where

C : γ-ray peak counts,
N : atomic number of target nuclide,
σ : activation cross section measured,
φ : neutron flux at the irradiation position,
ε : detection efficiency of γ-ray peak,
Iγ : γ-ray emission probability per disintegration,

λ : decay constant of induced radioactivity,

t_i : irradiation time,

t_c : cooling time,

t_m : measuring time of γ-ray,

All cross section values were obtained relative to the standard reaction cross section of $^{27}Al(n,\alpha)^{24}Na$ (ENDF/B-V)[3].

2.1 Experimental

2.1.1 Neutron Irradiation and Fluence Monitoring

The d-T neutrons were generated by an intense 14 MeV neutron source facility (OKTAVIAN) at Osaka University. Incident d^+ beam energy and intensity were 300 keV and about 5 mA, respectively. A pneumatic sample transport system as shown in Fig. 1 was used for the irradiation of samples. The distance between the T-target and the irradiation position was 15 cm. Transfer time was about 2 s. The angles of the irradiation position to the d^+ beam were 0°, 50°, 75°, 105°, 125° and 155°, which covered the neutron energies ranging from 14.9 to 13.4 MeV. Another pneumatic tube set at -105° was used to examine the arrangement of the pneumatic tubes. If the pneumatic tubes are well symmetrically set with respect to the incident deuteron beams, the measured neutron energy at -105° should show good agreement with one at 105° (see Fig. 2). When strongly induced activities are required, an additional tube set at -22.5° and at 1.5 cm was used. Typical neutron fluxes at each position are shown in Fig. 3. The neutron flux at 75° is a little low owing to neutron scattering with the rotating T-target assembly.

The neutron flux at the sample position was measured with use of the substandard $^{27}Al(n,p)^{27}Mg$ ($T_{1/2}$=9.46 min) reaction, whose cross sections were determined by referring to the standard $^{27}Al(n,\alpha)^{24}Na$ (ENDF/B-V)[3]. The samples were sandwiched between two aluminum foils of 10 mm × 10 mm × 0.2 mm thick. The standard cross section of $^{27}Al(n,\alpha)$ is shown in Table 3. Good statistics for fluence monitoring can be achieved in reasonably short measuring time by using the $^{27}Al(n,p)$ reaction instead of $^{27}Al(n,\alpha)$. The use of the substandard $^{27}Al(n,p)$ reaction brought only an additional uncertainty of 0.5% to final results.

The effective reaction energy of incident neutrons at each irradiation position was determined by the ratio of the $^{90}Zr(n,2n)^{89}Zr(3.27d)$[4] and $^{93}Nb(n,2n)^{92m}Nb(10.15d)$[5] cross sections (Zr/Nb method[6]). Since

each position of the pneumatic tubes is mutually arranged in good accuracy, the effective d^+ energy was chosen as a fitting parameter in the relativistic calculation of the d-T neutron energy. A fitting result obtained for E_d = 130 keV is shown in Fig. 2. The uncertainty in the neutron energy is estimated to be ± 50 keV.

Samples of separated isotope and natural element were used. Foil samples were rectangular-shaped 10 mm × 10 mm and 0.1 ~ 0.2 mm thick. Powder samples were wrapped in powder papers (each sample size: 10 mm × 10 mm and about 1 mm thick, sample masses: 30 ~ 90 mg). The specification of the samples used are shown in Table 4 and Table 5.

2.1.2 Activity Measurement

Gamma-rays emitted from the irradiated sample and monitor aluminum foils were measured with 12% HPGe (1.75 keV FWHM at 1333 keV) and 16% HPGe (2.00 keV), respectively. Each detector was covered with a 5 mm thick acrylic absorber in order to reduce β-rays. The peak efficiency calibration of the detectors at 5 cm was accomplished by using sources of ^{24}Na, ^{56}Co, ^{133}Ba, ^{152}Eu and ^{154}Eu. Corrections for true coincidence sums were applied. The errors in the efficiency curves are estimated to be 1.5% above 300 keV, 3% between 300 and 80 keV, and 5% below 80 keV. The characteristics of Ge detectors used are shown in Table 6.

To measure efficiently the weakly induced activities, the samples were put on the absorber surface (source-to-detector distance is 5 mm). To convert the efficiency at 5 mm to the one at 5 cm, calibration measurements were carried out at both distances by using extra samples irradiated at 1.5 cm from the neutron source with rather strong neutron flux. This method improved the detection efficiency by a factor of about 7. This calibration procedure brought an additional error of 1.0% to the results.

Peak areas of γ-rays are evaluated by summing all recorded counts in the channel interval {C-3σ, C+3σ} and subtracting the background counts (N_B), where C is the position of the peak center and σ is FWHM. N_B is given by $(6\sigma) \times (N_L + N_H)/2$, where N_L and N_H are the average counts of 5 channels in the vicinity of (C-3σ) and that in the vicinity of (C+3σ), respectively. This summing method is similar to that by Debertin and Schötzig[7]. The uncertainty from the peak area evaluation is estimated to be 0.5%.

2.1.3 Decay Data

In Table 7, measured reactions and associated decay data[8] of the half-life ($T_{1/2}$), the γ-ray energy (Eγ) and the absolute intensity in photons per disintegration (Iγ) are listed together with the Q values.

2.1.4 Corrections

The following principal corrections in deducing cross sections were made:

1) fluctuation of the neutron flux during the irradiation,
2) contribution of scattered low energy neutrons,
3) true coincidence sum,
4) random coincidence sum,
5) deviation in the measuring position coming from different thickness of each sample,
6) self-absorption of γ-ray in the sample material,
7) interfering reaction producing activities emitting γ-ray with same energy of interest.

The detailed procedures are described elsewhere[1,2].

2.1.5 Error Estimation

The total errors (δ_t) were derived by combining the experimental error (δ_e) and the error of nuclear data (δ_r) in quadratic:

$$\delta_t^2 = \delta_e^2 + \delta_r^2 \ .$$

Estimated major sources of the errors are listed in Table 8. When good counting statistics were achieved, the experimental error and the total error were 1.7% and 3.5%, respectively. The main error sources are due to the γ-ray detection efficiency and the standard $^{27}Al(n,\alpha)^{24}Na$ reaction cross section. In some cases the errors of the γ-ray emission probability or the half-life are dominant.

2.2 Results

Numerical data tables of the cross sections are given in Table 9 and graphs are given in Fig. 4. In the figures only experimental errors (δ_e) are shown.

Generally speaking, previous data obtained in the wide energy range of 13-15 MeV show fairly good agreement with the present results, while some of previous data obtained at one energy point are much different from the present results. This discrepancy might result from short sample-to-neutron source distance and large amounts of irradiation samples of the previous works, because available neutron sources in those works were weak. JENDL-3 shows agreement with the present data for $^{50}Ti(n,p)$, $^{54}Cr(n,\alpha)$ and $^{64}Ni(n,\alpha)$ within 10% and for $^{25}Mg(n,p)$, $^{29}Si(n,p)$ and $^{54}Cr(n,p)$ within 30%. The discrepancy shown in Fig. 4.16 for the $^{107}Ag(n,p)^{107m}Pd$ reaction results from the difference of the definition of the cross section; JENDL-3 gives the cross section for $^{107}Ag(n,p)^{107m+g}Pd$ while the present work gives the ground state formation cross section.

In our previous work of $^{26}Mg(n,\alpha)^{23}Ne$[2], the ^{26}MgO powder sample was used. Hence there was a possibility that some of induced activity of ^{23}Ne leaked from the irradiated sample. In this work, a natural metal plate of Mg was used to reduce the possibility of leakage. Present cross section values are higher by a factor of about 2 in comparison with the previous ones.

In appendix 1, the singles γ-ray spectra of samples irradiated by 14 MeV neutrons are shown.

3. Measurement of Half-lives

In the procedure to deduce the cross sections, the half-life value is one of the important decay data. It is therefore required that the half-life values are precise and reliable. Most of the values previously published have been obtained with GM counters, ionization chambers, proportional counters and scintillation counters about 20 years ago. On the other hand, works with the Ge detectors having the excellent energy resolution are very scarce. In order to improve the precision and the reliability of the half-life values, the Ge detectors were used.

3.1 Experimental

The γ-rays were measured with the Ge detector in the spectrum multi-scaling mode. Decay was followed for about 10 times the half-life at

Generally speaking, previous data obtained in the wide energy range of 13-15 MeV show fairly good agreement with the present results, while some of previous data obtained at one energy point are much different from the present results. This discrepancy might result from short sample-to-neutron source distance and large amounts of irradiation samples of the previous works, because available neutron sources in those works were weak. JENDL-3 shows agreement with the present data for $^{50}Ti(n,p)$, $^{54}Cr(n,\alpha)$ and $^{64}Ni(n,\alpha)$ within 10% and for $^{25}Mg(n,p)$, $^{29}Si(n,p)$ and $^{54}Cr(n,p)$ within 30%. The discrepancy shown in Fig. 4.16 for the $^{107}Ag(n,p)^{107m}Pd$ reaction results from the difference of the definition of the cross section; JENDL-3 gives the cross section for $^{107}Ag(n,p)^{107m+g}Pd$ while the present work gives the ground state formation cross section.

In our previous work of $^{26}Mg(n,\alpha)^{23}Ne$[2], the ^{26}MgO powder sample was used. Hence there was a possibility that some of induced activity of ^{23}Ne leaked from the irradiated sample. In this work, a natural metal plate of Mg was used to reduce the possibility of leakage. Present cross section values are higher by a factor of about 2 in comparison with the previous ones.

In appendix 1, the singles γ-ray spectra of samples irradiated by 14 MeV neutrons are shown.

3. Measurement of Half-lives

In the procedure to deduce the cross sections, the half-life value is one of the important decay data. It is therefore required that the half-life values are precise and reliable. Most of the values previously published have been obtained with GM counters, ionization chambers, proportional counters and scintillation counters about 20 years ago. On the other hand, works with the Ge detectors having the excellent energy resolution are very scarce. In order to improve the precision and the reliability of the half-life values, the Ge detectors were used.

3.1 Experimental

The γ-rays were measured with the Ge detector in the spectrum multi-scaling mode. Decay was followed for about 10 times the half-life at

equal intervals of 1/3 to 1/6 of the half-life. The ^{133}Ba (or ^{137}Cs, ^{170}Tm) source and a constant-pulser with a rate of 60 cps were simultaneously measured together with the short-lived activity for the correction of the pile-up and the dead time losses (source method, constant-pulser method). The initial counting rates were always kept to be less than 9×10^3 cps. Data points were analyzed by a least squares fitting. The detailed procedures are described elsewhere[9].

3.2 Source Preparation

Sources of ^{51}Ti, ^{60m}Co, ^{91g}Mo and ^{94}Y were produced by 14 MeV neutron bombardments. Sources of ^{51}Ti, ^{60m}Co, ^{88}Rb, ^{108}Ag and ^{109m}Pd produced by thermal neutron irradiation at the TRIGA-II reactor of Rikkyo University (100 kW).

3.3 Results

The results are summarized in Table 10 together with production reactions, γ-rays followed, reference sources for corrections and previous works[8]. As an example, γ-ray spectrum and the decay curve in the decay of 4.3 min ^{104}Rh are shown in Fig. 5 and Fig. 6, respectively. The results are shown in Fig. 7 together with previous works taken from ref. 8. In Fig. 8, difference of previous half-life values from the present ones in percent. Previous values shorter than about 10 min are larger than the present results in general. These might be due to insufficient corrections. It was likely to start the measurements at too high counting rates in order to get good statistics.

4. Summary

The activation cross sections were measured on 16 reactions producing short-lived nuclei in the neutron energy range of 13.4 to 14.9 MeV for F, Mg, Si, Ti, Ni, Ga, Rb, Sr and Ag. Seven half-lives of short-lived nuclei were measured by applying both the source and pulser methods, which showed systematically smaller values than the previous ones in the range shorter than 10 min as a whole.

equal intervals of 1/3 to 1/6 of the half-life. The ^{133}Ba (or ^{137}Cs, ^{170}Tm) source and a constant-pulser with a rate of 60 cps were simultaneously measured together with the short-lived activity for the correction of the pile-up and the dead time losses (source method, constant-pulser method). The initial counting rates were always kept to be less than 9×10^3 cps. Data points were analyzed by a least squares fitting. The detailed procedures are described elsewhere[9].

3.2 Source Preparation

Sources of ^{51}Ti, ^{60m}Co, ^{91g}Mo and ^{94}Y were produced by 14 MeV neutron bombardments. Sources of ^{51}Ti, ^{60m}Co, ^{88}Rb, ^{108}Ag and ^{109m}Pd produced by thermal neutron irradiation at the TRIGA-II reactor of Rikkyo University (100 kW).

3.3 Results

The results are summarized in Table 10 together with production reactions, γ-rays followed, reference sources for corrections and previous works[8]. As an example, γ-ray spectrum and the decay curve in the decay of 4.3 min ^{104}Rh are shown in Fig. 5 and Fig. 6, respectively. The results are shown in Fig. 7 together with previous works taken from ref. 8. In Fig. 8, difference of previous half-life values from the present ones in percent. Previous values shorter than about 10 min are larger than the present results in general. These might be due to insufficient corrections. It was likely to start the measurements at too high counting rates in order to get good statistics.

4. Summary

The activation cross sections were measured on 16 reactions producing short-lived nuclei in the neutron energy range of 13.4 to 14.9 MeV for F, Mg, Si, Ti, Ni, Ga, Rb, Sr and Ag. Seven half-lives of short-lived nuclei were measured by applying both the source and pulser methods, which showed systematically smaller values than the previous ones in the range shorter than 10 min as a whole.

Acknowledgements

This work was performed under the contract between Nagoya University and Japan Atomic Energy Research Institute.

The authors wish to express their sincere thanks to Dr. Y. Nakajima of the JAERI Nuclear Data Center. They are also grateful to Prof. K. Sumita for his support to this work and Messrs. H. Sugimoto, M. Datemichi and S. Yoshida for the operation of the OKTAVIAN accelerator. Messrs. A. Osa, T. Ikuta, A. Taniguchi and A. Hosoya are appreciated for help in this experiment.

References

1) T. Katoh, K. Kawade and H. Yamamoto: JAERI-M 89-083 (1989) (in Japanese).
2) K. Kawade, H. Yamamoto, T. Yamada, T. Katoh, T. Iida and A. Takahashi: JAERI-M 90-171 (1990).
3) "Evaluated Neutron Data File, ENDF/B-V", ENDF/B Summary Documentation, compiled by R. Kinsey, ENDF-201, 3rd edition, Brookhaven Laboratory (1979).
4) A. Pavlik, G. Winkler, H. Vonach, A. Paulsen and H. Liskien: J. Phys. G; Nucl. Phys. 8, 1283 (1982).
5) D.R. Nethaway: J. Inorg. Nucl. Chem. 40, 1285 (1978).
6) V.E. Lewis and K.J. Zieba: Nucl. Instr. Meth. 174, 141 (1980).
7) K. Debertin and U. Schötzig: Nucl. Instr. Meth. 140, 337 (1977).
8) E. Browne, R.B. Firestone and V.S. Shirley: "Table of Radioactive Isotopes", John Wiley & Sons, New York (1986).
9) M. Miyachi, H. Ukon, M. Shibata, Y. Gotoh, H. Yamamoto, K. Kawade, T. Katoh, T. Iida and A. Takahashi: Proc. Nucl. Data for Sci. and Tech. (1988, Mito) p.897.
10) K. Kawade, H. Miyahara, K. Hara and Y. Kasugai: KURRI-TR-341 (1990) p.30 (in Japanese).

Acknowledgements

This work was performed under the contract between Nagoya University and Japan Atomic Energy Research Institute.

The authors wish to express their sincere thanks to Dr. Y. Nakajima of the JAERI Nuclear Data Center. They are also grateful to Prof. K. Sumita for his support to this work and Messrs. H. Sugimoto, M. Datemichi and S. Yoshida for the operation of the OKTAVIAN accelerator. Messrs. A. Osa, T. Ikuta, A. Taniguchi and A. Hosoya are appreciated for help in this experiment.

References

1) T. Katoh, K. Kawade and H. Yamamoto: JAERI-M 89-083 (1989) (in Japanese).
2) K. Kawade, H. Yamamoto, T. Yamada, T. Katoh, T. Iida and A. Takahashi: JAERI-M 90-171 (1990).
3) "Evaluated Neutron Data File, ENDF/B-V", ENDF/B Summary Documentation, compiled by R. Kinsey, ENDF-201, 3rd edition, Brookhaven Laboratory (1979).
4) A. Pavlik, G. Winkler, H. Vonach, A. Paulsen and H. Liskien: J. Phys. G; Nucl. Phys. 8, 1283 (1982).
5) D.R. Nethaway: J. Inorg. Nucl. Chem. 40, 1285 (1978).
6) V.E. Lewis and K.J. Zieba: Nucl. Instr. Meth. 174, 141 (1980).
7) K. Debertin and U. Schötzig: Nucl. Instr. Meth. 140, 337 (1977).
8) E. Browne, R.B. Firestone and V.S. Shirley: "Table of Radioactive Isotopes", John Wiley & Sons, New York (1986).
9) M. Miyachi, H. Ukon, M. Shibata, Y. Gotoh, H. Yamamoto, K. Kawade, T. Katoh, T. Iida and A. Takahashi: Proc. Nucl. Data for Sci. and Tech. (1988, Mito) p.897.
10) K. Kawade, H. Miyahara, K. Hara and Y. Kasugai: KURRI-TR-341 (1990) p.30 (in Japanese).

Table 1 Measured activation cross sections

Reaction[a]	$T_{1/2}$	Reaction[a]	$T_{1/2}$
$^{19}F(n,p)^{19}O$	26.91s	$^{64}Ni(n,\alpha)^{61}Fe$	5.98m
$^{25}Mg(n,p)^{25}Na$	59.6s	$^{69}Ga(n,\alpha)^{66}Cu$	5.10m
$^{26}Mg(n,\alpha)^{23}Ne$	37.6s	$^{87}Rb(n,2n)^{86m}Rb$	1.017m
$^{29}Si(n,p)^{29}Al$	6.56m	$(n,\alpha)^{84m}Br$	6.0m
$(n,np)^{28}Al$	2.241m	$^{86}Sr(n,p)^{86m}Rb$	1.017m
$^{50}Ti(n,p)^{50m+g}Sc$	1.710m	$^{87}Sr(n,np)^{86m}Rb$	1.017m
$^{54}Cr(n,p)^{54}V$	49.8s	$^{107}Ag(n,p)^{107m}Pd$	21.3s
$(n,np)^{53}V$	1.61m		
$(n,\alpha)^{51}Ti$	5.76m		

[a] (n,np) means [(n,d) + (n,n'p) + (n,pn)].

Table 2 Measured half-lives

Nuclide						
^{51}Ti	^{60m}Co	^{88}Rb	^{91m}Mo	^{94}Y	^{108}Ag	^{109m}Pd
(5.8m)	(10m)	(18m)	(15m)	(19m)	(2.4m)	(4.7m)

Table 3 Cross section of $^{27}Al(n,\alpha)^{24}Na$ reaction[a]

En(MeV)	Cross section(mb)
14.96	113.42
14.92	113.93
14.84	114.97
14.71	116.65
14.53	118.97
14.32	121.28
14.10	123.63
13.95	125.02
13.81	125.93
13.68	126.77
13.55	127.62
13.33	128.60

[a] taken from ENDF/B-V[3]
Uncertainty is ±3% for all values.

Table 4 Samples of separated isotope

Sample	Chemical form	Enrichment (%)	Weight (mg)	Reaction	Impurity[a] (%)
^{25}Mg	MgO	98.814	60	^{25}Mg(n,p)	24(0.963), 25(0.223)
^{29}Si	SiO_2	95.65	60	^{29}Si(n,p) (n,np)	28(4.12) , 30(0.23)
^{50}Ti	TiO_2	96.75	50	^{50}Ti(n,p)$^{m+g}$	46(0.27), 47(0.25) 48(2.40), 49(0.33)
^{54}Cr	Cr_2O_3	96.78	30	^{54}Cr(n,p) (n,np) (n,α)	50(0.06), 52(2.26) 53(0.90)
^{64}Ni	Ni	97.92	30	^{64}Zn(n,α)	58(0.92) , 60(0.73) 61(0.05) , 62(0.38)
^{69}Ga	Ga_2O_3	99.79	70	^{69}Ga(n,α)	71(0.21)
^{87}Rb	RbCl	97.32	90	^{87}Rb(n,2n)^m_m (n,α)^m_m	85(2.68)
^{86}Sr	$SrCO_3$	97.02	80	^{86}Zn(n,p)^m	84(0.08), 87(0.78) 88(2.12)
^{87}Sr	$SrCO_3$	91.26	90	^{87}Zn(n,np)	84(0.01), 86(0.82) 88(7.91)
^{107}Ag	Ag	99.09	70	^{107}Ag(n,p)^m	109(0.91)

[a] A(x) means mass nummber A with atomic percent x.

Table 5 Samples of natural abundance

Sample	Chemical form	Purity (%)	Weight (mg)	Reaction	Abundance (%)
F	$(CF_2)n$	99	190	^{19}F(n,p)	19(100)
Mg	Mg	99.999	330	^{26}Mg(n,α)	24(78.99),25(10.0), 26(11.01)

Table 6 Ge detectors used for cross section measurement

Detector	Volume (cm^3)	Efficiency (%)	FWHM (keV)	Object of measurement
Vertical HPGe	60	12	1.75	short-lived nuclei
Horizontal HPGe	89	16	2.00	Al monitor foil (^{27}Mg)
Horizontal HPGe	113	23	2.00	^{92m}Nb, ^{89}Zr for Neutron Energy

Table 7 Reactions and decay parameters[a)]

Reaction[b)]	$T_{1/2}$	Eγ (keV)	Iγ (%)	Q(MeV)[c)]
$^{19}F(n,p)^{19}O$	26.91s	197.1	95.9(21)	-4.04
$^{25}Mg(n,p)^{25}Na$	59.6s	585.0	12.96(71)	-3.05
$^{26}Mg(n,\alpha)^{23}Ne$	37.6s	439.9	32.9(10)	-5.41
$^{29}Si(n,p)^{29}Al$	6.56m	1273.4	91.3	-2.90
$(n,np)^{28}Al$	2.241m	1779.0	100	-12.33
$^{50}Ti(n,p)^{50m+g}Sc$	1.710m	523.8	88.7(18)	-6.11
$^{54}Cr(n,p)^{54}V$	49.8s	834.8	97.1(17)	-6.26
$(n,np)^{53}V$	1.61m	1006.2	90(2)	-12.37
$(n,\alpha)^{51}Ti$	5.76m	320.1	93.0(4)	-1.56
$^{64}Ni(n,\alpha)^{61}Fe$	5.98m	298.0	22.2(28)	-2.53
$^{69}Ga(n,\alpha)^{66}Cu$	5.10m	1039.4	9.12(14)[d)]	2.58
$^{87}Rb(n,2n)^{86m}Rb$	1.017m	556.1	98.19(1)	-10.48
$(n,\alpha)^{84m}Br$	6.0(m)	424.3	100(10)	-1.49
$^{86}Sr(n,p)^{86m}Rb$	1.017m	556.1	98.19(1)	-1.55
$^{87}Sr(n,np)^{86m}Rb$	1.017m	556.1	98.19(1)	-9.98
$^{107}Ag(n,p)^{107m}Pd$	21.3s	214.9	69.0(20)	0.53
$^{27}Al(n,\alpha)^{24}Na$[e)]	14.959h	1368.6	99.994(3)	-3.13
$^{27}Al(n,p)^{27}Mg$[f)]	9.46m	843.8	72.0(4)[d)]	-1.83

a) taken from ref. 8.

b) (n,np) means [(n,d)+(n,n'p)+(n,pn)].

c) Q(n,n'p) is given here. Q(n,d)=Q(n,n'p)+2.225MeV.

d) taken from ref.10.

e) Standard reaction(ENDF/B-V) used in this work.

f) Secondary conventional reaction used for short-lived nuclei.

Table 8 Principal sources of uncertainty in the measured cross sections

Experimetal error (δe)	
Source of error	Uncertainty(%)
Counting statistics	0.5 - 40
Sample mass including purity	0.1
Neutron flux fluctuation	<0.1 (20% of correction)
Gamma-peak area evaluation	0.5
Detector efficiency	1.5($E\gamma$ >300 keV), 3(300 - 80 keV), 5($E\gamma$ <80 keV)
Efficiency calibration at 0.5 and 5 cm	1.0
Correction for true coincidence sum	<0.3
Correction for random coincidence sum	<0.4
Correction for sample thickness	0.2 - 0.6 (20% of correction)
Correction for self-absorption of γ-rays	0 - 0.2 (20% of correction)
Correction for low energy neutrons	0 - 5 (30~40% of correction)
Secondary reference cross section for $^{27}Al(n,p)^{27}Mg$	0.5 (only statistics)

Error of nuclear data (δr)	
Source of error	Uncertainty(%)
Reference cross section for $^{27}Al(n,\alpha)^{24}Na$(ENDF/B-V)	3.0
Absolute γ-ray intensity	0 - 13
Half-life	0 - 5

Table 9(a) Activation cross section of short-lived nuclei

$^{19}F(n,p)^{19}O(26.91s)$					$^{25}Mg(n,p)^{25}Na(59.6S)$			
En(MeV)	σ(mb)	δ_e(%)	δ_r(%)	δ_t(%)	σ(mb)	δ_e(%)	δ_r(%)	δ_t(%)
14.87	17.8	3.6	3.7	5.2	62.6	4.7	6.3	7.9
14.58	18.6	3.6	3.7	5.2	63.7	4.6	6.3	7.8
14.28	19.4	3.7	3.7	5.2	67.3	4.9	6.3	8.0
18.88	19.5	3.6	3.7	5.2	63.3	4.3	6.3	7.7
13.65	20.8	3.6	3.7	5.2	63.4	4.4	6.3	7.7
13.40	22.7	3.6	3.7	5.2	62.0	4.4	6.3	7.7
$^{26}Mg(n,\alpha)^{23}Ne(37.6s)$					$^{29}Si(n,p)^{29}Al(6.56m)$			
En(MeV)	σ(mb)	δ_e(%)	δ_r(%)	δ_t(%)	σ(mb)	δ_e(%)	δ_r(%)	δ_t(%)
14.87	55.4	3.7	4.3	5.6	130.8	1.9	3.0	3.6
14.58	57.5	3.8	4.3	5.7	131.6	1.9	3.0	3.6
14.28	56.4	4.0	4.3	5.8	131.7	2.1	3.0	3.7
18.88	57.4	4.2	4.3	6.0	132.7	1.9	3.0	3.6
13.65	59.8	3.7	4.3	5.7	130.6	2.0	3.0	3.6
13.40	58.3	3.6	4.3	5.6	125.6	1.9	3.0	3.6
$^{29}Si(n,np)^{28}Al(2.241m)$					$^{50}Ti(n,p)^{50m+g}Sc(1.710m)$			
En(MeV)	σ(mb)	δ_e(%)	δ_r(%)	δ_t(%)	σ(mb)	δ_e(%)	δ_r(%)	δ_t(%)
14.87	24.7	2.8	3.0	4,2	14.4	4.0	3.6	5.4
14.58	17.9	3.2	3.0	4.4	13.5	4.1	3.6	5.5
14.28	13.2	3.7	3.0	4.8	13.0	4.5	3.6	5.7
18.88	10.3	3.5	3.0	4.6	12.0	4.2	3.6	5.5
13.65	8.6	3.8	3.0	4.8	10.6	4.2	3.6	5.5
13.40	6.0	4.4	3.0	5.0	10.2	4.6	3.6	5.8

* δ_e : experimental error , δ_r : error of nuclear data , $\delta_t^2 = \delta_e^2 + \delta_r^2$
* Error of neutron energy is estimated as about 50 keV.

Table 9(b) Activation cross section of short-lived nuclei

$^{54}Cr(n,p)^{54}V(49.8s)$					$^{54}Cr(n,np)^{53}V(1.61m)$			
En(MeV)	σ(mb)	δ_e(%)	δ_r(%)	δ_t(%)	σ(mb)	δ_e(%)	δ_r(%)	δ_t(%)
14.87	21.3	5.3	3.6	6.3	3.3	13	3.8	14
14.58	21.6	5.6	3.6	6.6	3.2	14	3.8	15
14.28	20.8	6.9	3.6	7.8	1.5	27	3.8	27
18.88	17.5	6.0	3.6	7.0	1.4	24	3.8	24
13.65	13.4	6.4	3.6	7.3	0.7	36	3.8	36
13.40	15.0	6.7	3.6	7.6	0.5	43	3.8	43

$^{54}Cr(n,\alpha)^{51}Ti(5.76m)$					$^{64}Ni(n,\alpha)^{61}Fe(5.98m)$			
En(MeV)	σ(mb)	δ_e(%)	δ_r(%)	δ_t(%)	σ(mb)	δ_e(%)	δ_r(%)	δ_t(%)
14.87	13.2	2.6	3.4	4.1	6.0	4.9	13.0	14
14.58	12.8	2.5	3.4	4.2	5.5	5.9	13.0	14
14.28	12.1	3.3	3.4	4.7	5.1	9.0	13.0	16
18.88	11.7	2.4	3.4	4.2	4.5	5.5	13.0	14
13.65	11.0	2.6	3.4	4.3	3.7	8.0	13.0	15
13.40	10.3	2.5	3.4	4.2	3.0	7.4	13.0	15

$^{69}Ga(n,\alpha)^{66}Cu(5.10m)$					$^{87}Rb(n,2n)^{86m}Rb(1.017m)$			
En(MeV)	σ(mb)	δ_e(%)	δ_r(%)	δ_t(%)	σ(mb)	δ_e(%)	δ_r(%)	δ_t(%)
14.87	20.7	5.9	3.4	6.8	527	1.7	3.0	3.5
14.58	21.7	6.3	3.4	7.1	559	1.7	3.0	3.5
14.28	19.6	9.6	3.4	10	508	1.8	3.0	3.5
18.88	23.5	5.6	3.4	6.6	460	1.7	3.0	3.5
13.65	24.0	6.2	3.4	7.1	478	1.7	3.0	3.5
13.40	22.0	5.3	3.4	6.3	463	1.7	3.0	3.5

* δ_e : experimental error , δ_r : error of nuclear data , $\delta_t^2 = \delta_e^2 + \delta_r^2$
* Error of neutron energy is estimated as about 50 keV.

Table 9(c) Activation cross section of short-lived nuclei

$^{87}Rb(n,\alpha)^{84m}Br(6.0m)$					$^{86}Sr(n,p)^{86m}Rb(1.017m)$			
En(MeV)	σ(mb)	δ_e(%)	δ_r(%)	δ_t(%)	σ(mb)	δ_e(%)	δ_r(%)	δ_t(%)
14.87	0.81	9.4	10	14	12.9	3.8	3.0	4.9
14.58	0.69	14	10	17	13.2	4.0	3.0	5.0
14.28	0.77	24	10	26	12.1	4.9	3.0	5.7
18.88	0.59	13	10	17	12.7	3.6	3.0	4.7
13.65	0.52	18	10	21	11.1	4.0	3.0	5.0
13.40	0.49	14	10	18	10.1	4.1	3.0	5.0

$^{87}Sr(n,np)^{86m}Rb(1.017m)$					$^{107}Ag(n,p)^{107m}Pd(21.3s)$			
En(MeV)	σ(mb)	δ_e(%)	δ_r(%)	δ_t(%)	σ(mb)	δ_e(%)	δ_r(%)	δ_t(%)
14.87	4.3	5.9	3.7	6.6	7.3	9.2	5.2	11
14.58	3.4	7.8	3.7	8.3	7.4	9.9	5.2	11
14.28	2.2	9.7	3.7	10	7.9	9.4	5.2	11
18.88	1.8	9.2	3.7	9.7	7.2	8.9	5.2	10
13.65	1.1	13	3.7	13	7.3	8.0	5.2	9.6
13.40	0.3	30	3.7	30	7.7	8.3	5.2	10

* δ_e : experimental error , δ_r : error of nuclear data , $\delta_t^2 = \delta_e^2 + \delta_r^2$
* Error of neutron energy is estimated as about 50 keV.

Table 10 Results of half-life measurement

Nuclide	Production reaction	Eγ (keV)	Reference[a] (Eγ in keV)	Half-life Present	Half-life Reference[b]
^{51}Ti	^{51}V(n,p) ^{50}Ti(n,γ)	320.1	^{57}Co (122.1)	5.759(9)m	5.80(3)m
^{60m}Co	^{60}Ni(n,p)^{m} ^{59}Co(n,γ)^{m}	58.6 1332.5	[c] ^{137}Cs(661.7)	10.424(20)m	10.47(2)m
^{88}Rb	^{87}Rb(n,γ)^{m}	898.0	^{137}Cs (661.7)	17.748(23)m	17.78(11)m
^{91g}Mo	^{92}Mo(n,2n)^{g}	511($\gamma^{\pm}$)	^{133}Ba (356.0)	15.473(34)m	15.49(1)m
^{94}Y	^{94}Zr(n,p)	918.8	^{137}Cs (661.7)	18.50(26)m	18.7(1)m
^{108}Ag	^{107}Ag(n,γ)	633.0	^{133}Ba (356.0)	2.353(9)m	2.37(1)m
^{109m}Pd	^{108}Pd(n,γ)^{m}	188.9	^{57}Co (122.1)	4.663(11)m	4.69(1)m

[a] These sources were used for corrections of dead-time and pile-up losses.

[b] taken from ref. 8.

[c] No source was used. Pulser was only used.

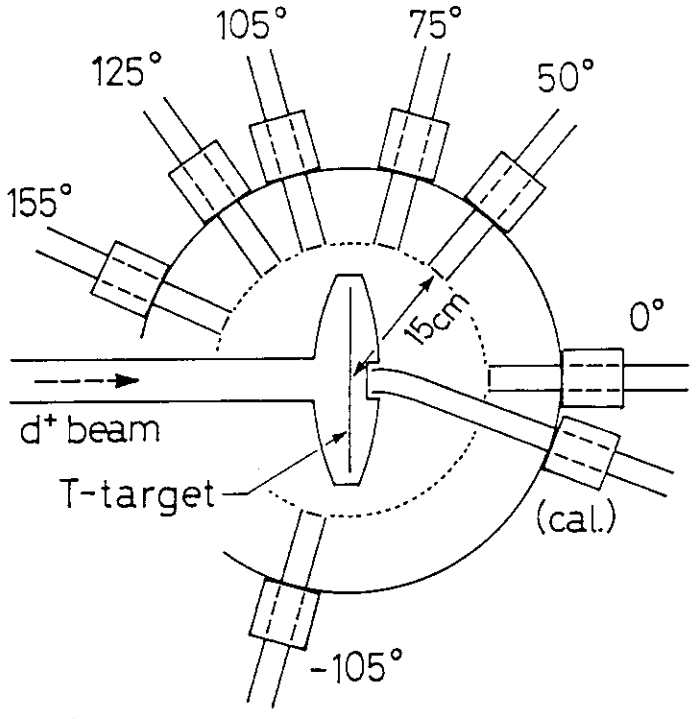

Fig. 1 Pneumatic sample transport system at OKTAVIAN.

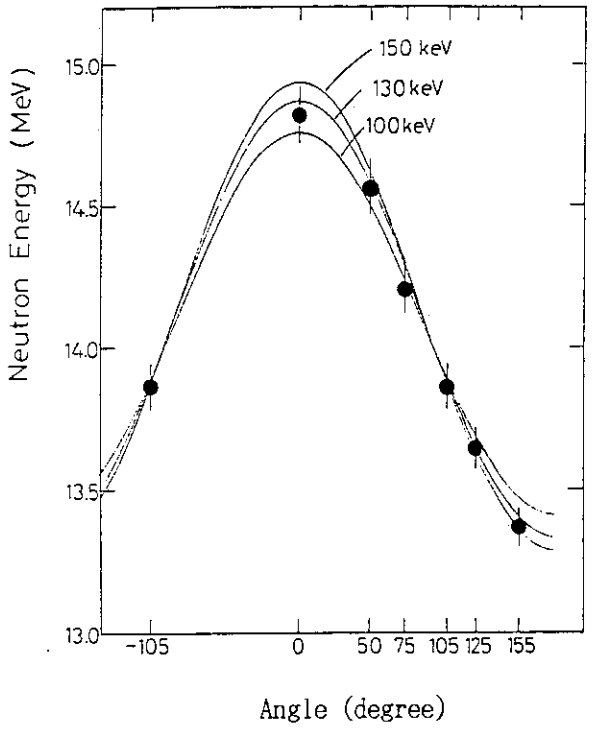

Fig. 2 Neutron flux at 15 cm.

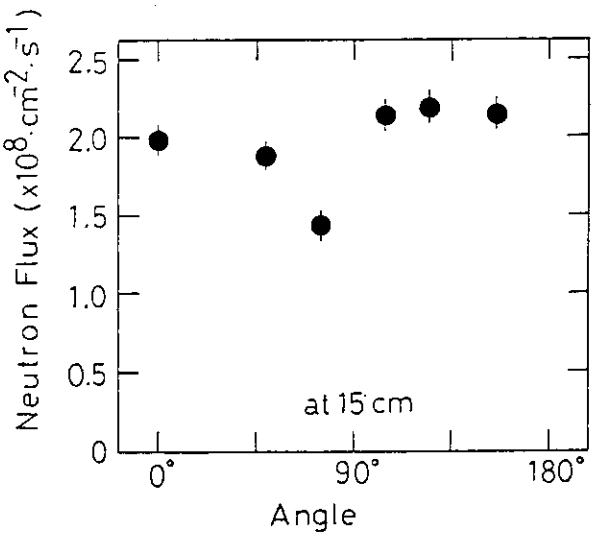

Fig. 3 Angular dependences of d-T neutron energy.

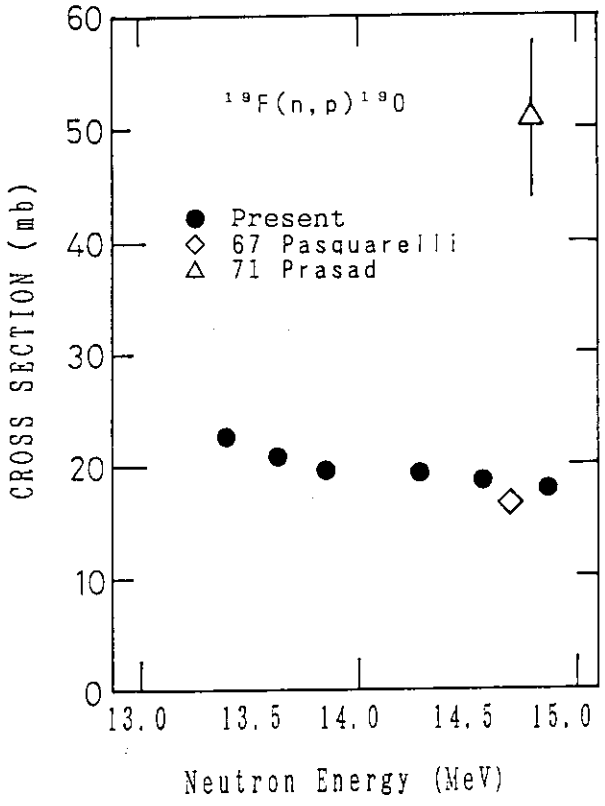

Fig. 4.1 Cross section of $^{19}F(n,p)^{19}O$.

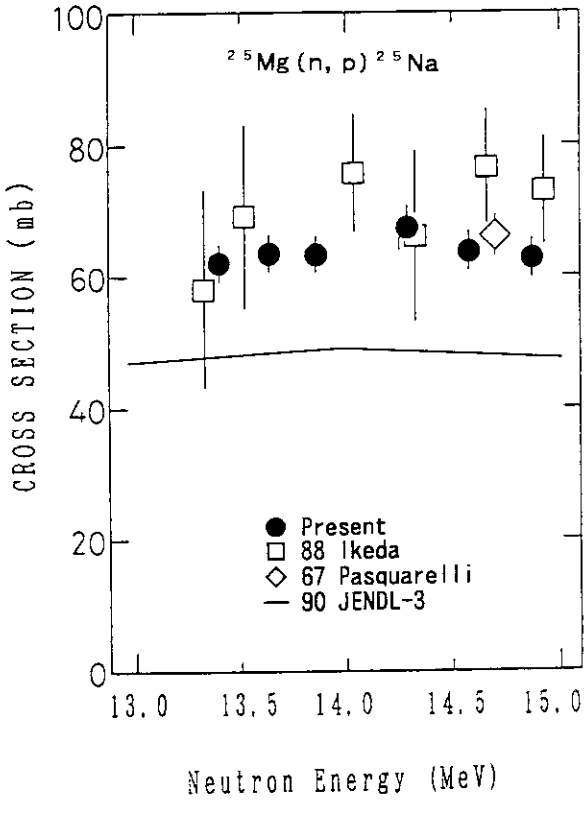

Fig. 4.2 Cross section of $^{25}Mg(n,p)^{25}Na$.

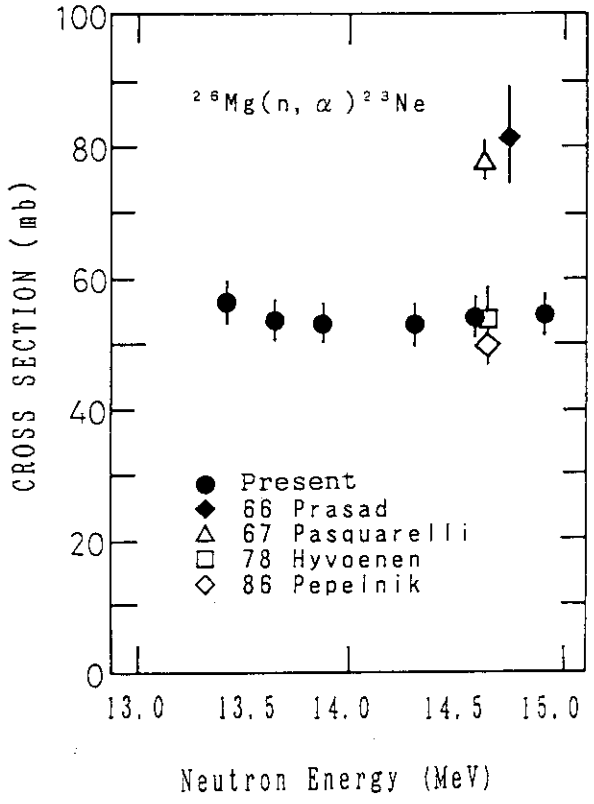

Fig. 4.3 Cross section of $^{26}Mg(n,\alpha)^{23}Ne$.

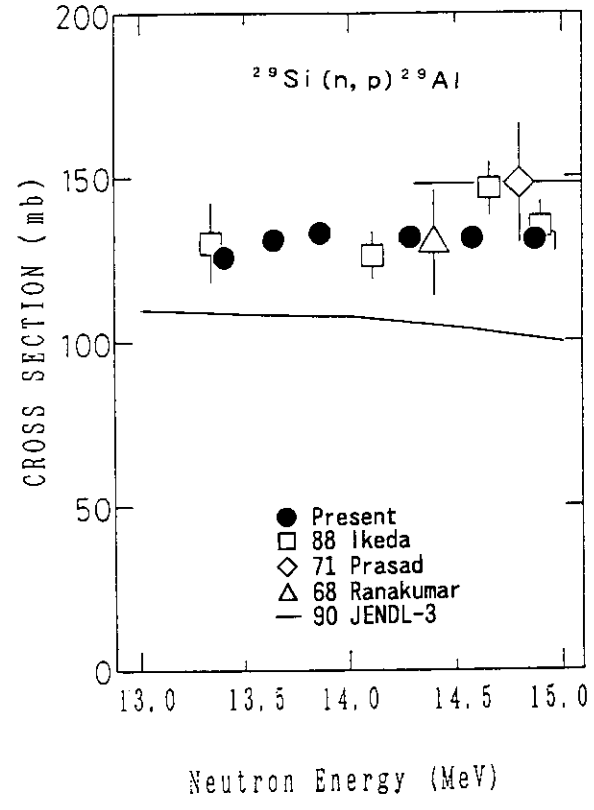

Fig. 4.4 Cross section of $^{29}Si(n,p)^{29}Al$.

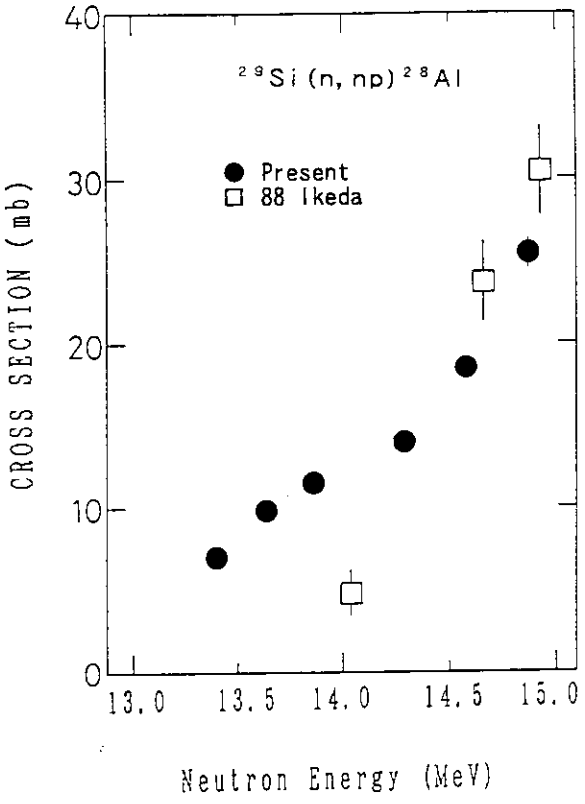

Fig. 4.5 Cross section of ^{29}Si(n,n'p)^{28}Al.

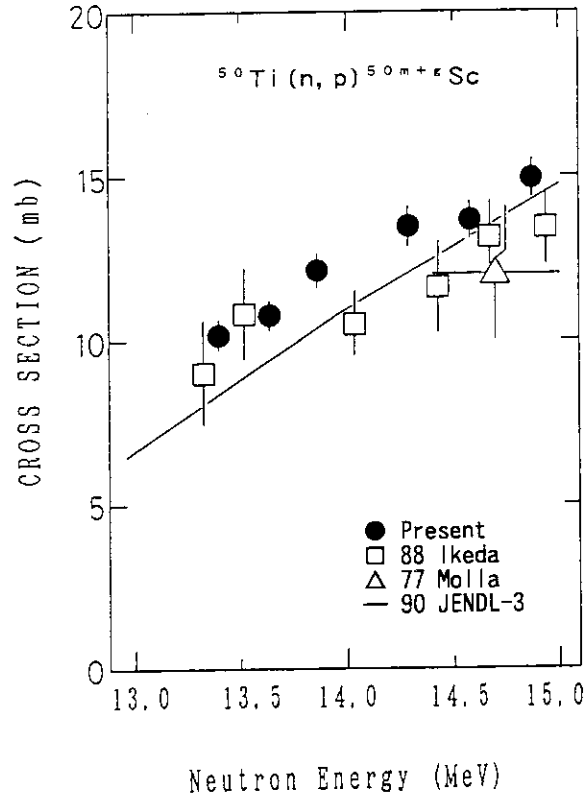

Fig. 4.6 Cross section of ^{50}Ti(n,p)$^{50m+g}$Sc.

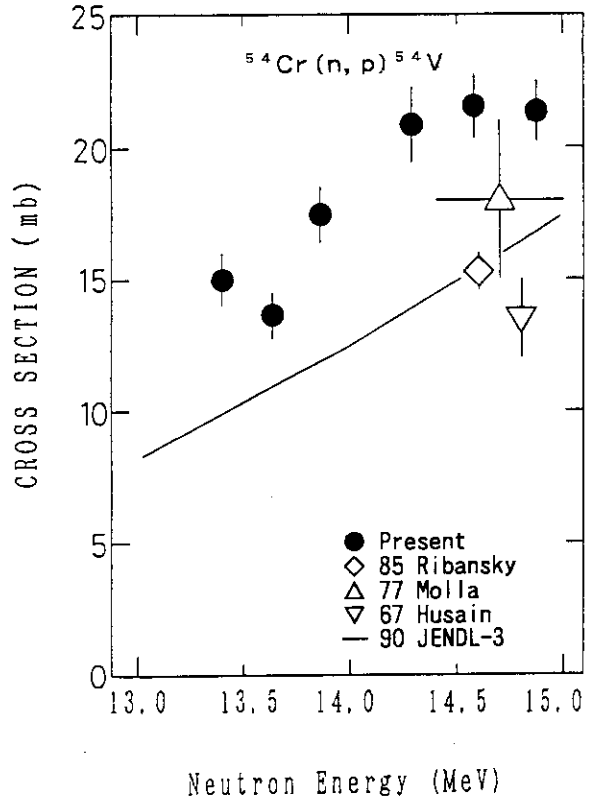

Fig. 4.7 Cross section of ^{54}Cr(n,p)^{54}V.

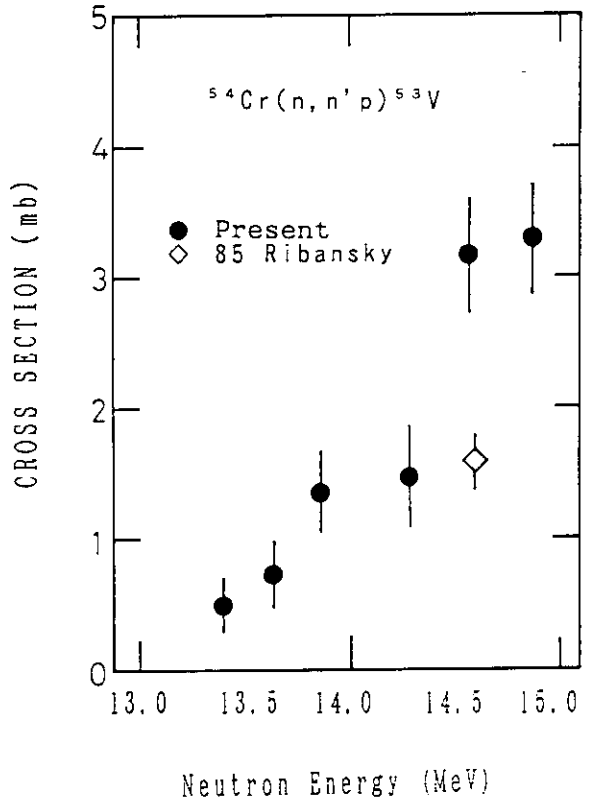

Fig. 4.8 Cross section of ^{54}Cr(n,n'p)^{53}V.

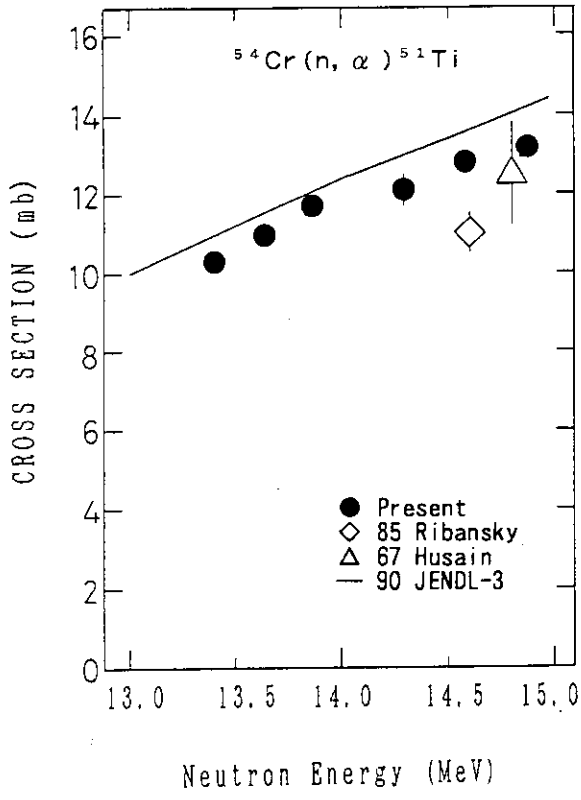

Fig. 4.9 Cross section of $^{54}Cr(n,\alpha)^{51}Ti$.

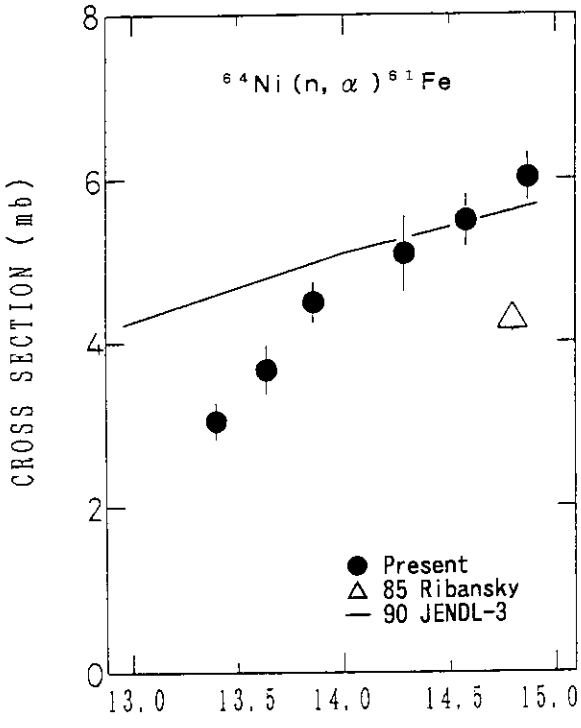

Fig. 4.10 Cross section of $^{64}Ni(n,\alpha)^{61}Fe$.

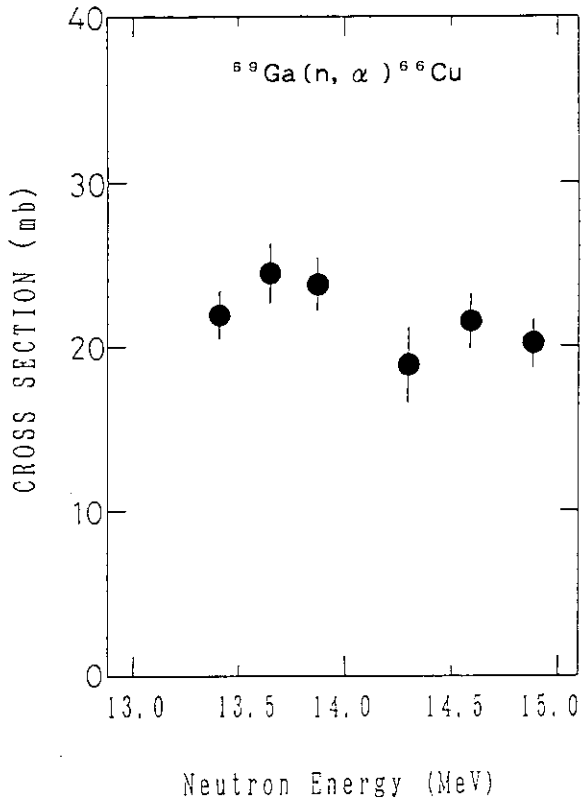

Fig. 4.11 Cross section of $^{69}Ga(n,\alpha)^{66}Cu$.

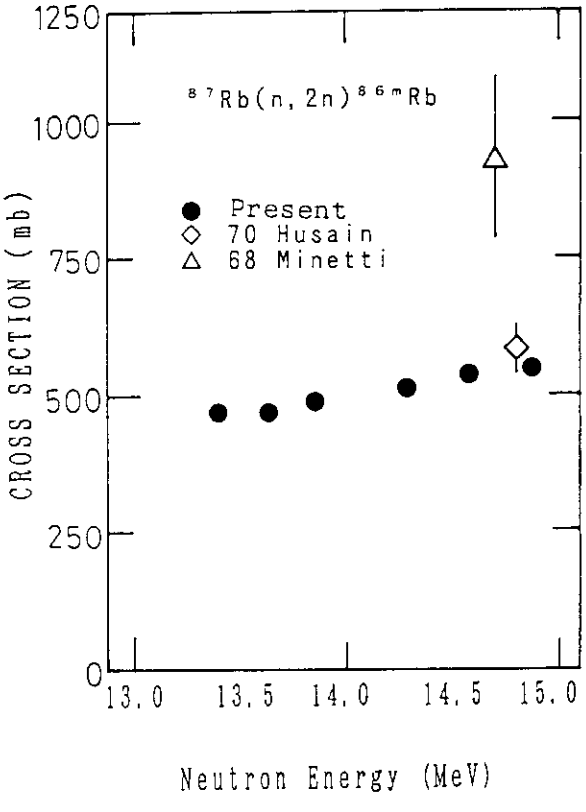

Fig. 4.12 Cross section of $^{87}Rb(n,2n)^{86m}Rb$.

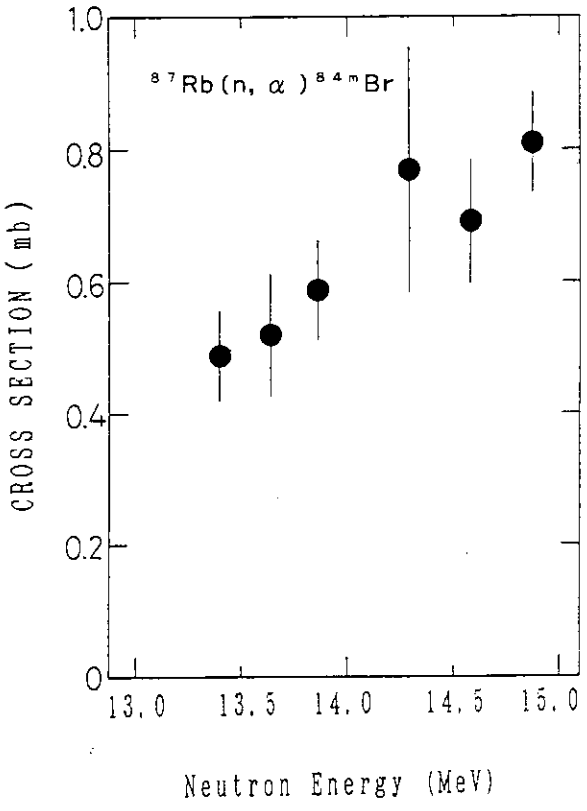

Fig. 4.13 Cross section of $^{87}Rb(n,\alpha)^{84m}Br$.

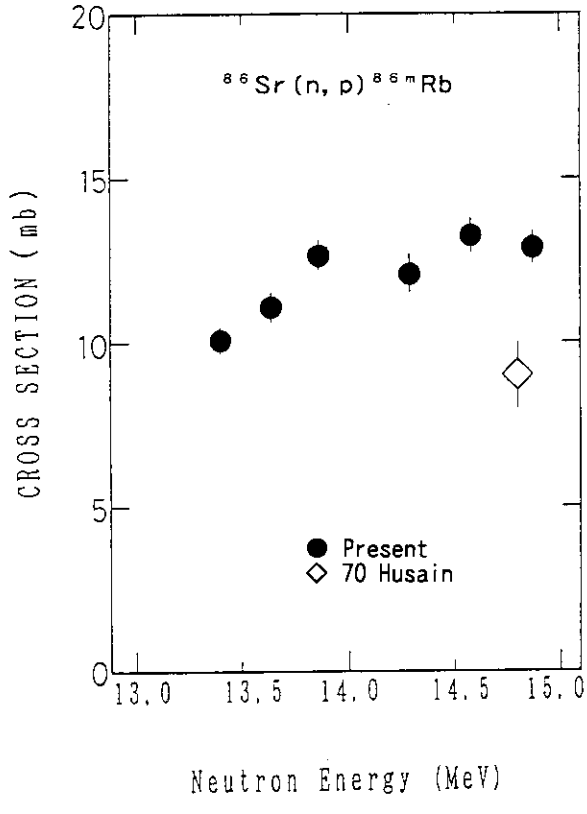

Fig. 4.14 Cross section of $^{86}Sr(n,p)^{86m}Rb$.

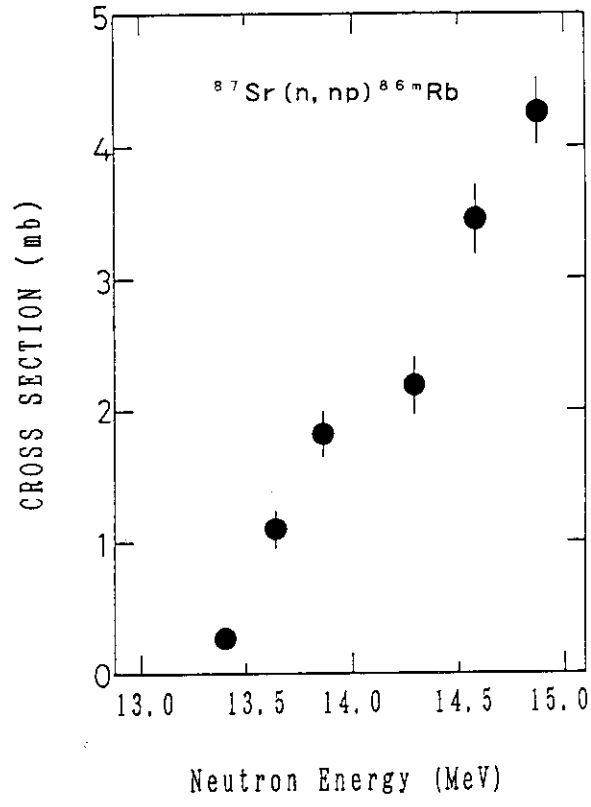

Fig. 4.15 Cross section of ^{87}Sr(n,n'p)^{86m}Rb.

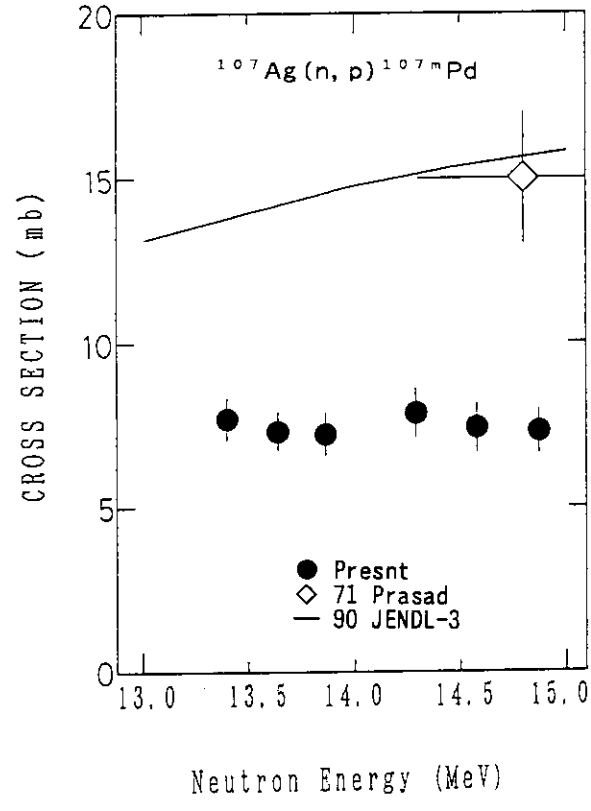

Fig. 4.16 Cross section of ^{107}Ag(n,p)^{107m}Pd.

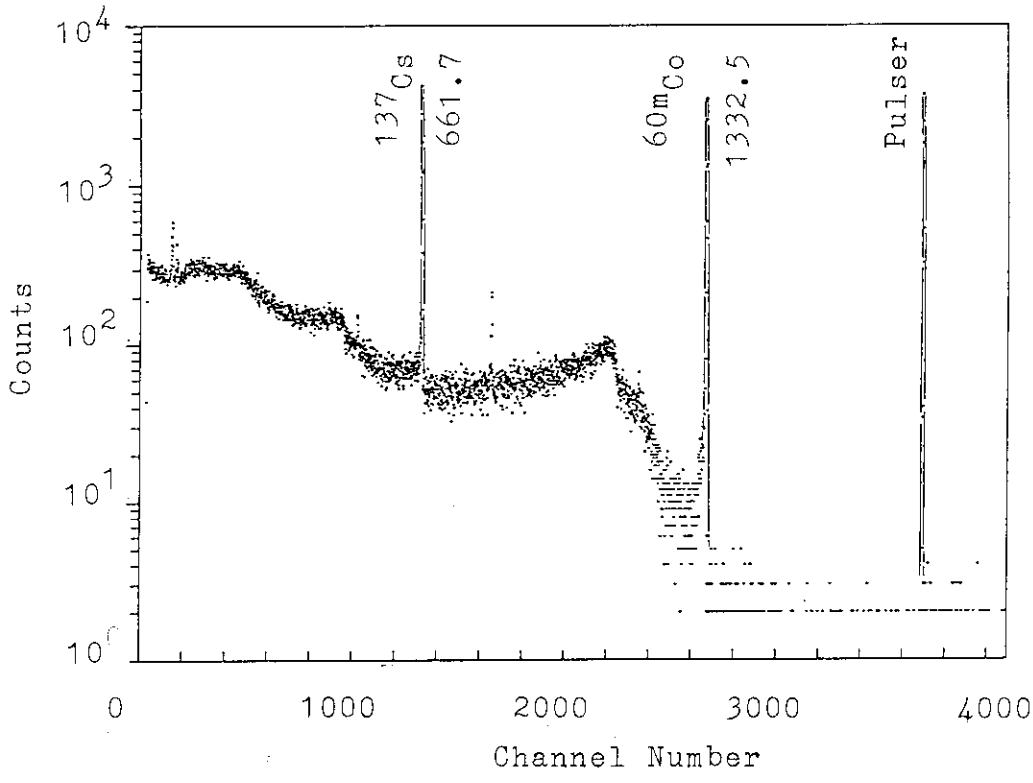

Fig. 5 Gamma-ray spectrum in the decay of ^{60m}Co. Gamma-rays from ^{137}Cs and signals of pulser were simultaneously measured for the correction of pile-up losses.

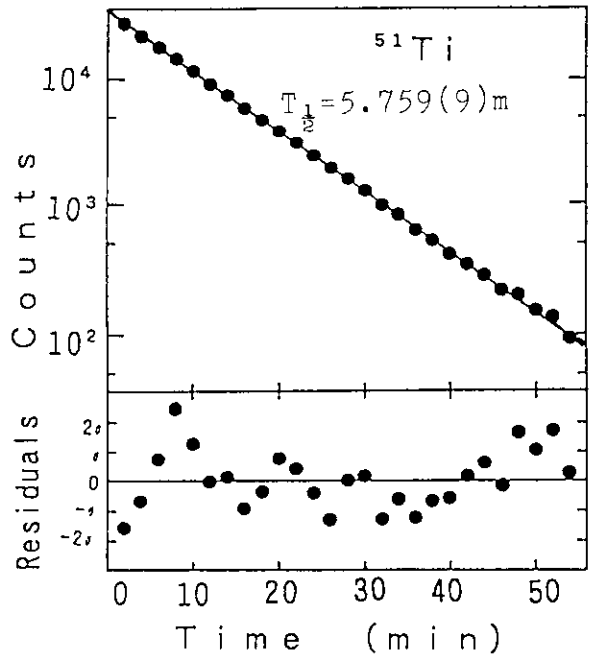

Fig. 6 Decay curve of 5.8 min ^{51}Ti and residuals obtained from a least squares fitting analysis.

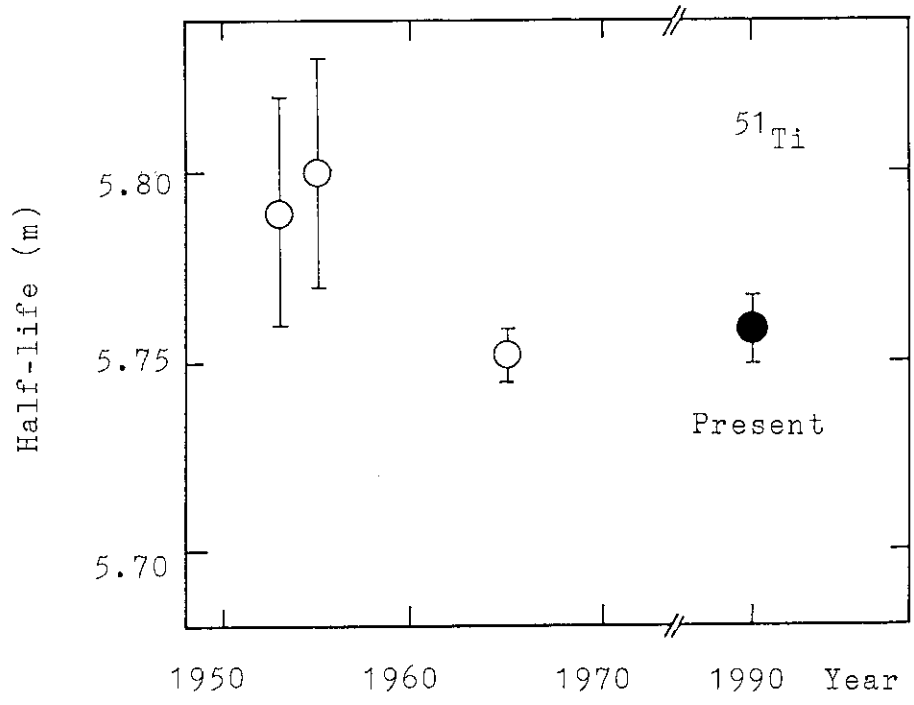

Fig. 7.1 Half-life of ^{51}Ti. Previous works are taken from ref. 8.

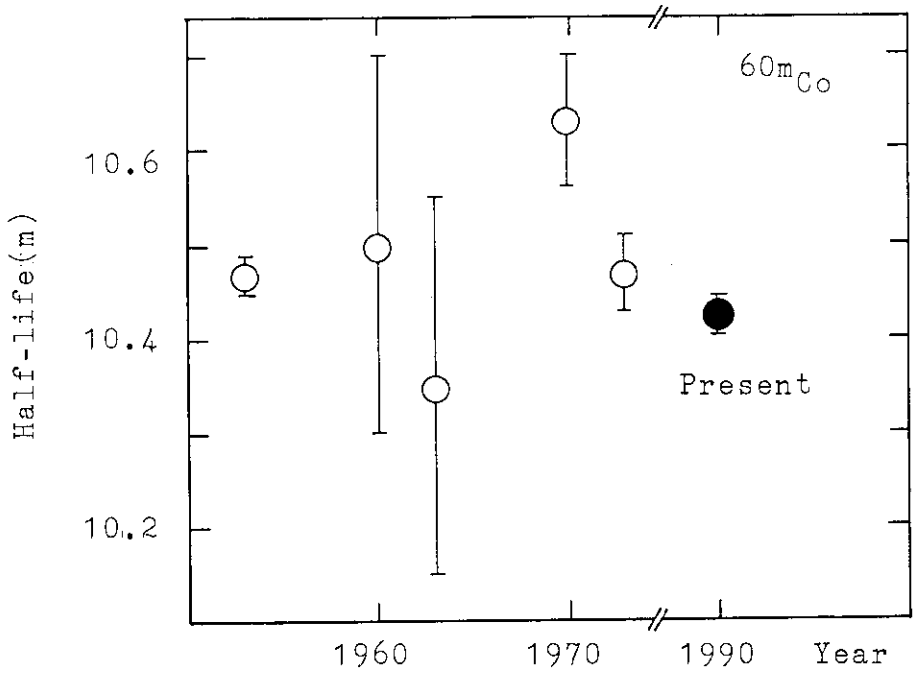

Fig. 7.2 Half-life of ^{60m}Co.

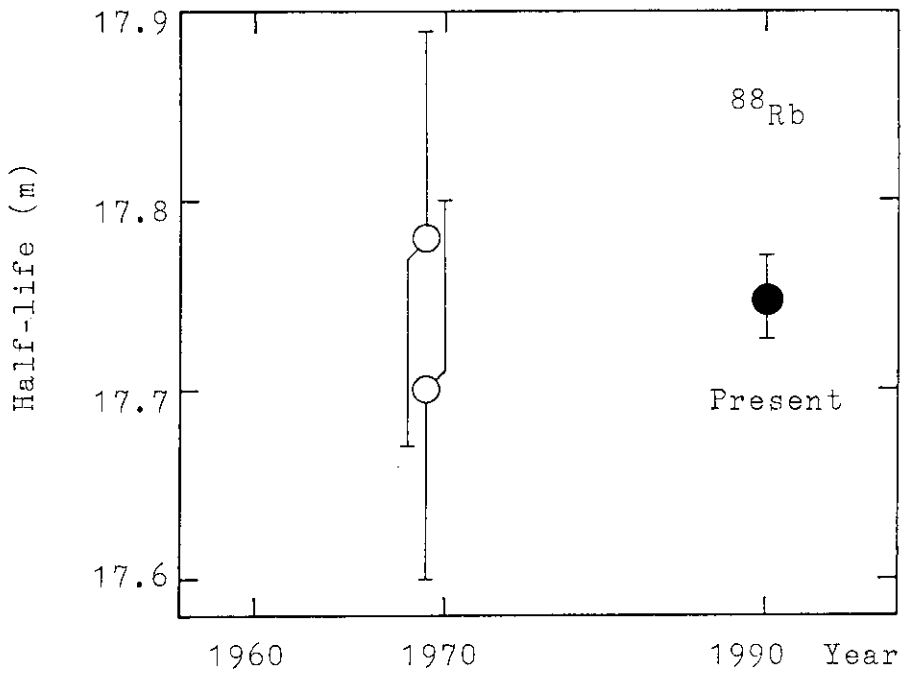

Fig. 7.3 Half-life of ^{88}Rb.

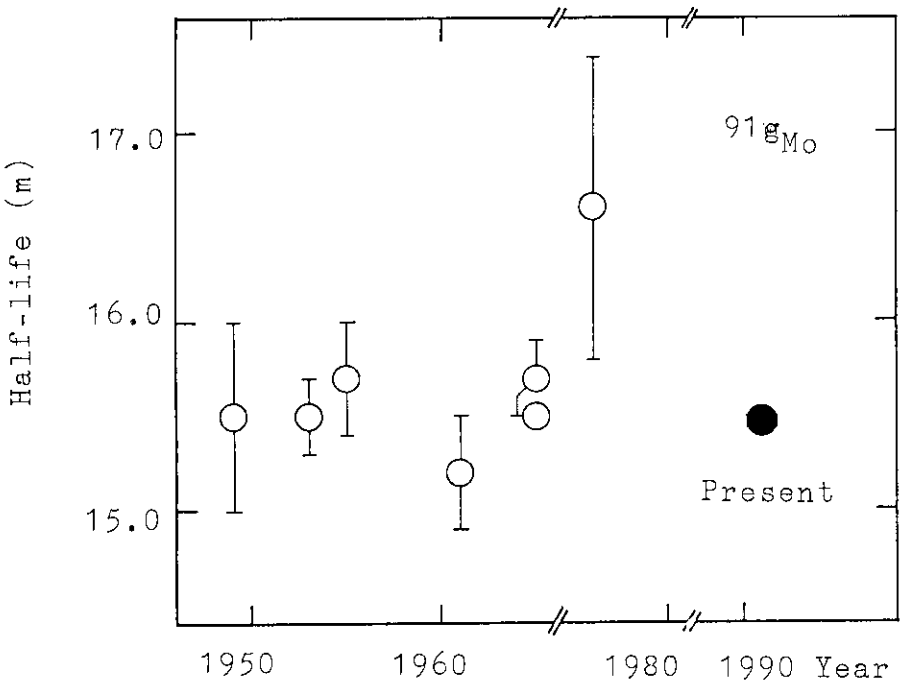

Fig. 7.4 Half-life of ^{91g}Mo.

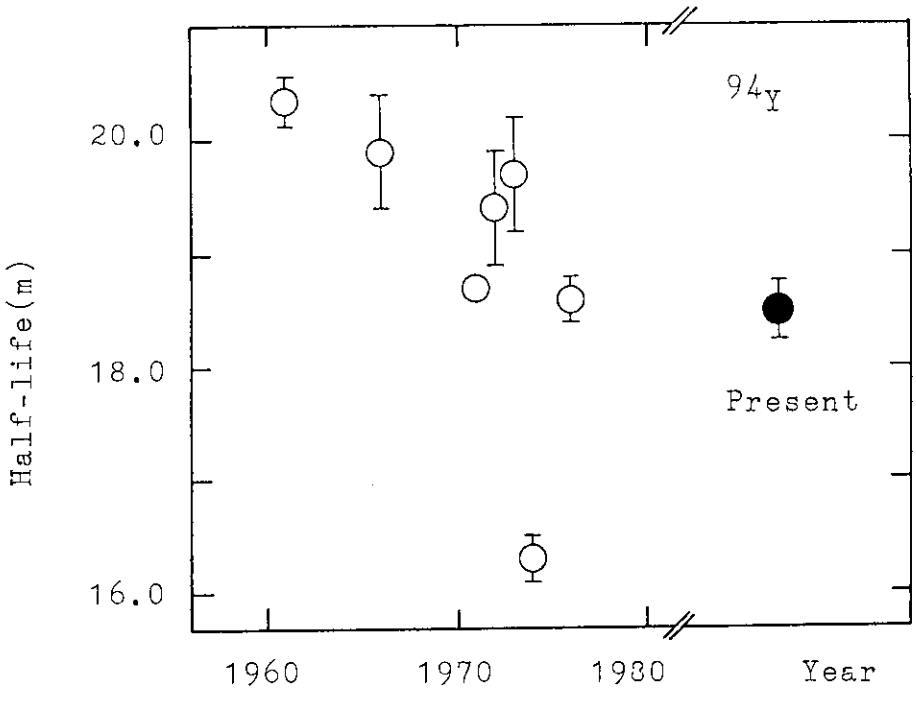

Fig. 7.5 Half-life of ^{94}Y.

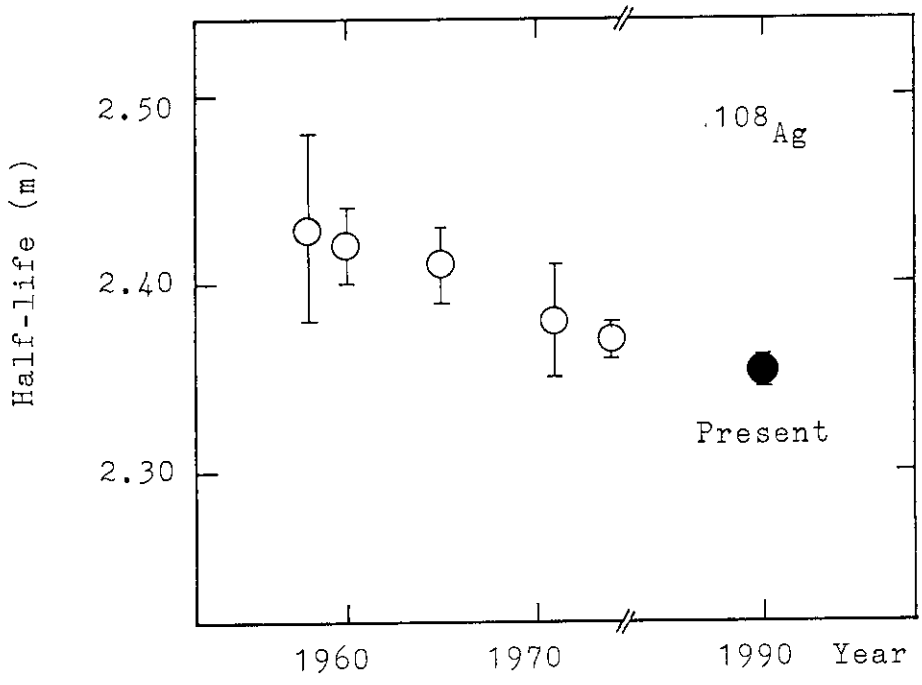

Fig. 7.6 Half-life of ^{108}Ag.

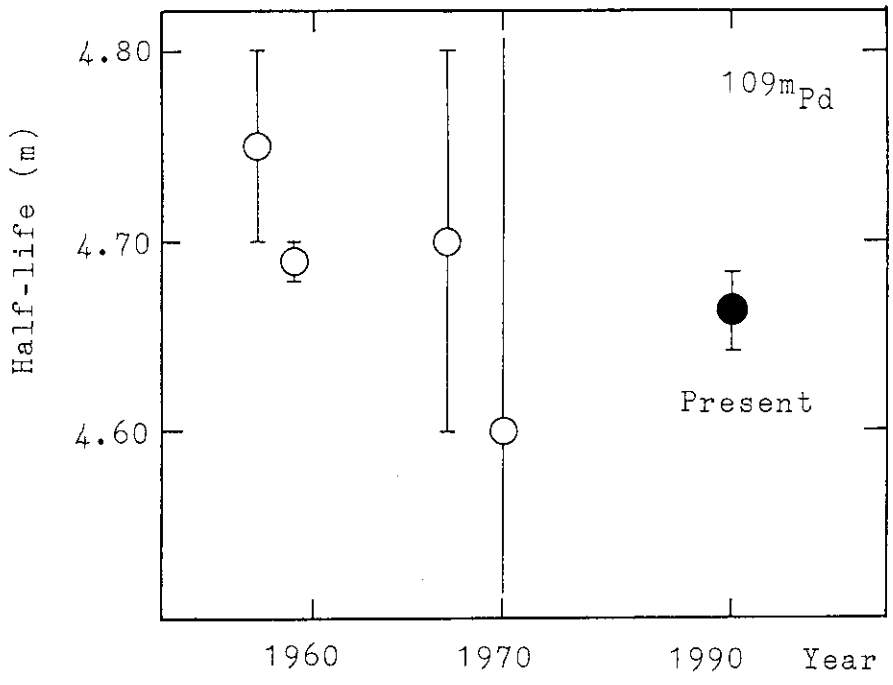

Fig. 7.7 Half-life of ^{109m}Pd.

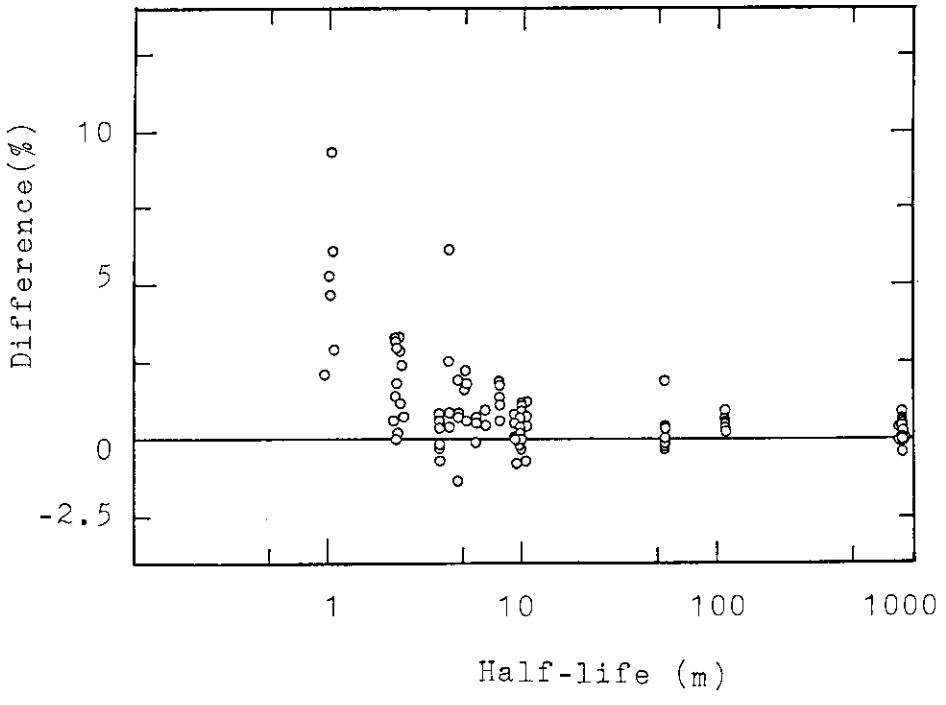

Fig. 8 Difference of previous half-lives from the present work in percent(%).

Appendix 1 Gamma-ray spectra of samples irradiated by 14.9 MeV neutrons are given in Fig. A.1.1 ~ 26.

EXPLANATION

Sample: ^{25}MgO(98.81%)	⇒ ①
Time: 300s-26s-180s	⇒ ②
●: ^{25}Mg(n,p)^{25}Na	⇒ ③
Det.: 12% HPGe	⇒ ④
Distance: 0.5cm	⇒ ⑤

① Sample(enrichment % for separated isotope, nat.:sample of natural abundance)
② Irradiation time-cooling time-measurement time
③ Reaction
④ Detector. Usually Ge detectors are covered with 5mm acrylic absorber.
⑤ Source-to-detector distance.

* Gamma-ray energies are in KeV. 511γ; 511keV annihilation γ-ray,
S.E.P.; single escape peak, D.E.P.; double escape peak.

Irradiated Samples	Page	Fig.A.1.X X=	Irradiated Samples	Page	Fig.1.X X=
$(CF_2)n$(nat.)		1,2	$^{69}Ga_2O_3$(99.79%)		15,16
^{25}MgO(98.814%)		3,4	^{87}RbCl(97.32%)		17,18
Mg(nat.)		5,6	$^{86}SrCO_3$(97.02%)		19,20
$^{29}SiO_2$(95.63%)		7,8	$^{87}SrCO_3$(91.26%)		21,22
$^{50}TiO_2$(96.75%)		9,10	^{107}Ag(99.09%)		23,24
$^{54}Cr_2O_3$(96.78%)		11,12	Zr(nat.)		25
^{64}Ni(97.92%)		13,14	Nb(nat.)		26

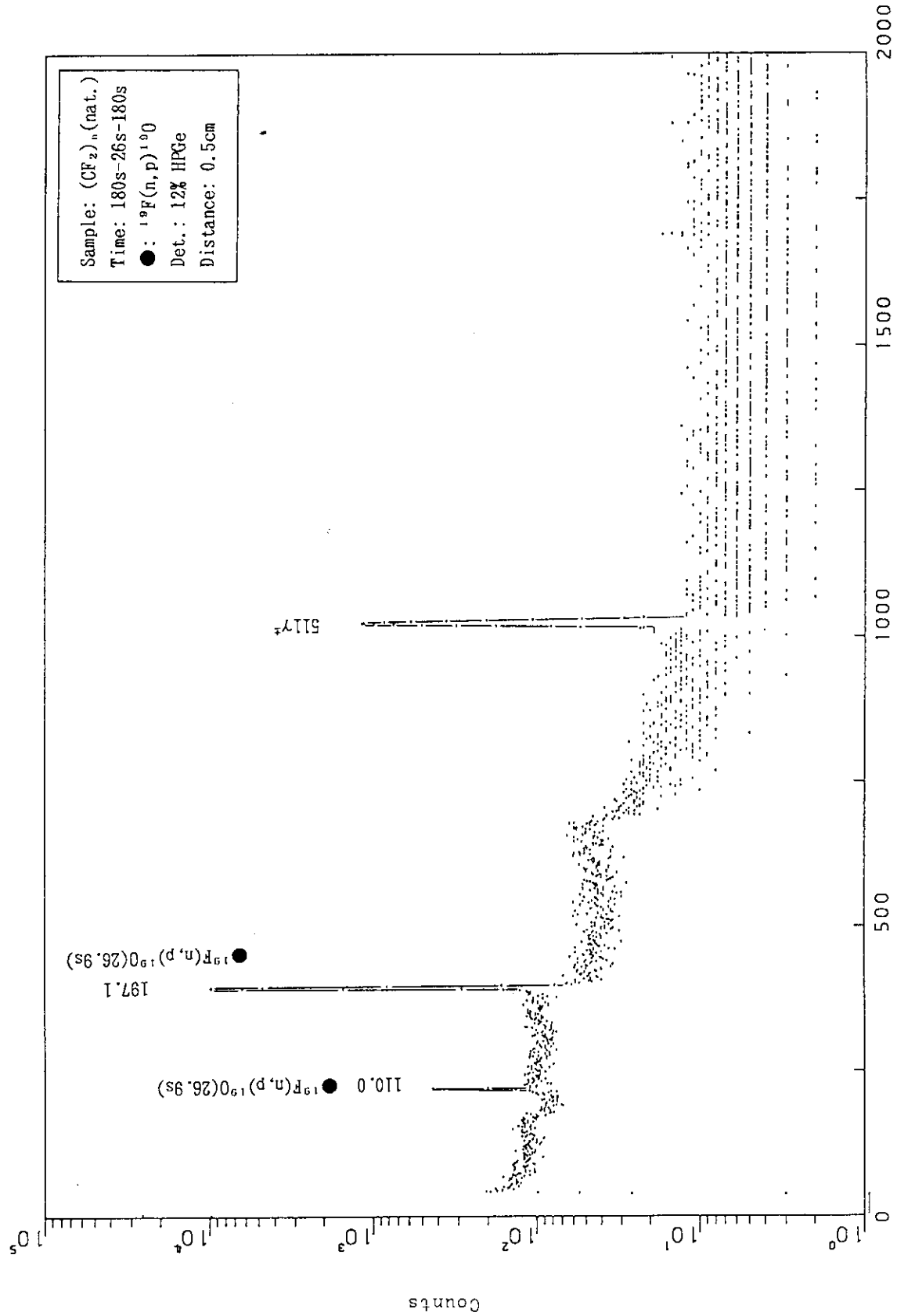
Sample: $(CF_2)_n$(nat.)
Time: 180s-26s-180s
●: $^{19}F(n,p)^{19}O$
Det.: 12% HPGe
Distance: 0.5cm
511γ±
197.1
●19F(n,p)19O(26.9s)
110.0
●19F(n,p)19O(26.9s)
Counts
Channel Number
0
500
1000
1500
2000

Fig. A.1.1

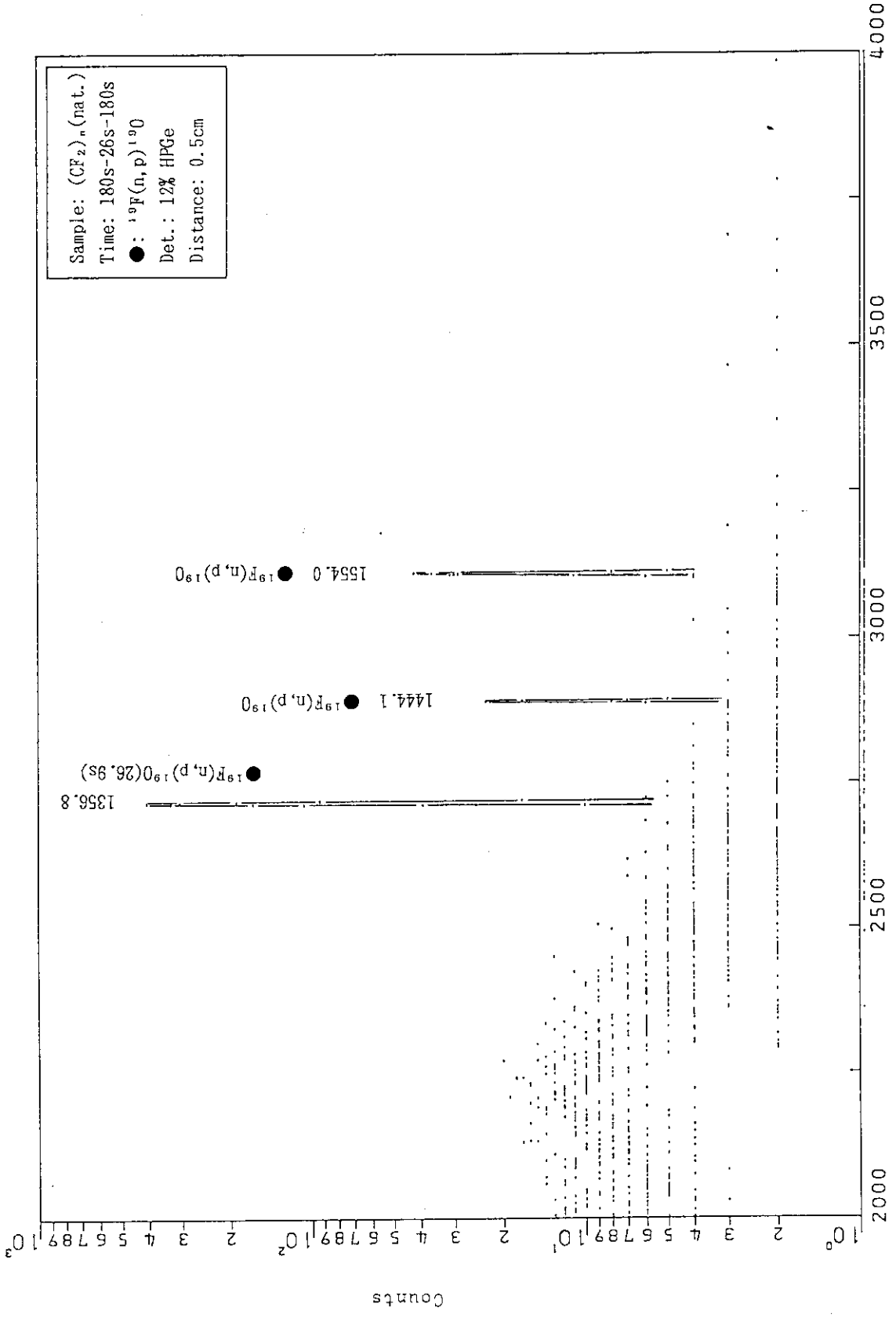
Sample: $(CF_2)_n$(nat.)
Time: 180s-26s-180s
●: $^{19}F(n,p)^{19}O$
Det.: 12% HPGe
Distance: 0.5cm
1356.8
●$^{19}F(n,p)^{19}O(26.9s)$
1444.1 ●$^{19}F(n,p)^{19}O$
1554.0 ●$^{19}F(n,p)^{19}O$
Counts
Channel Number

Fig. A.1.2

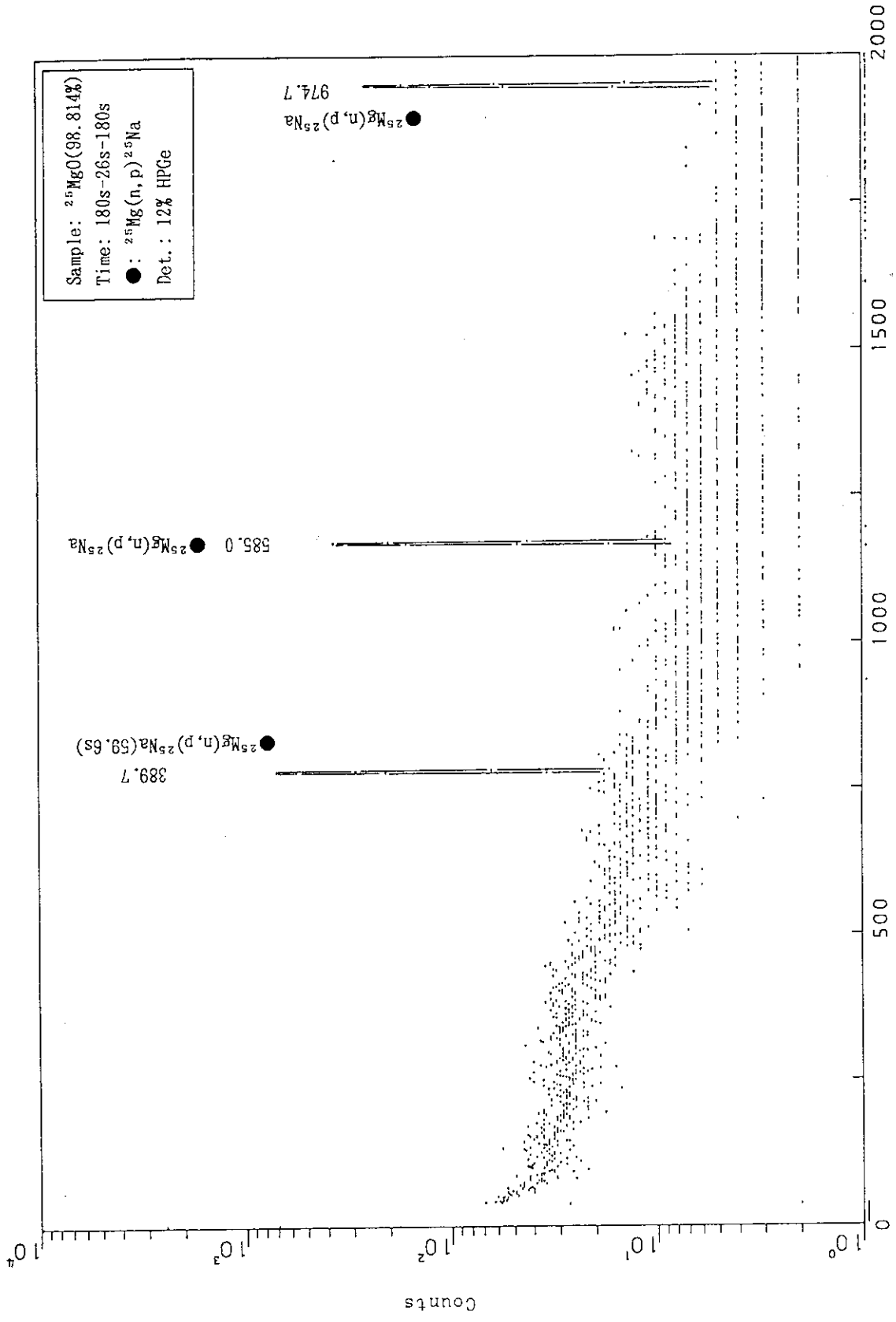
Sample: ^{25}MgO(98.814%)
Time: 180s-26s-180s
●: ^{25}Mg(n,p)^{25}Na
Det.: 12% HPGe
974.7
●^{25}Mg(n,p)^{25}Na
585.0
●^{25}Mg(n,p)^{25}Na
389.7
●^{25}Mg(n,p)^{25}Na(59.6s)
Counts
Channel Number

Fig. A.1.3

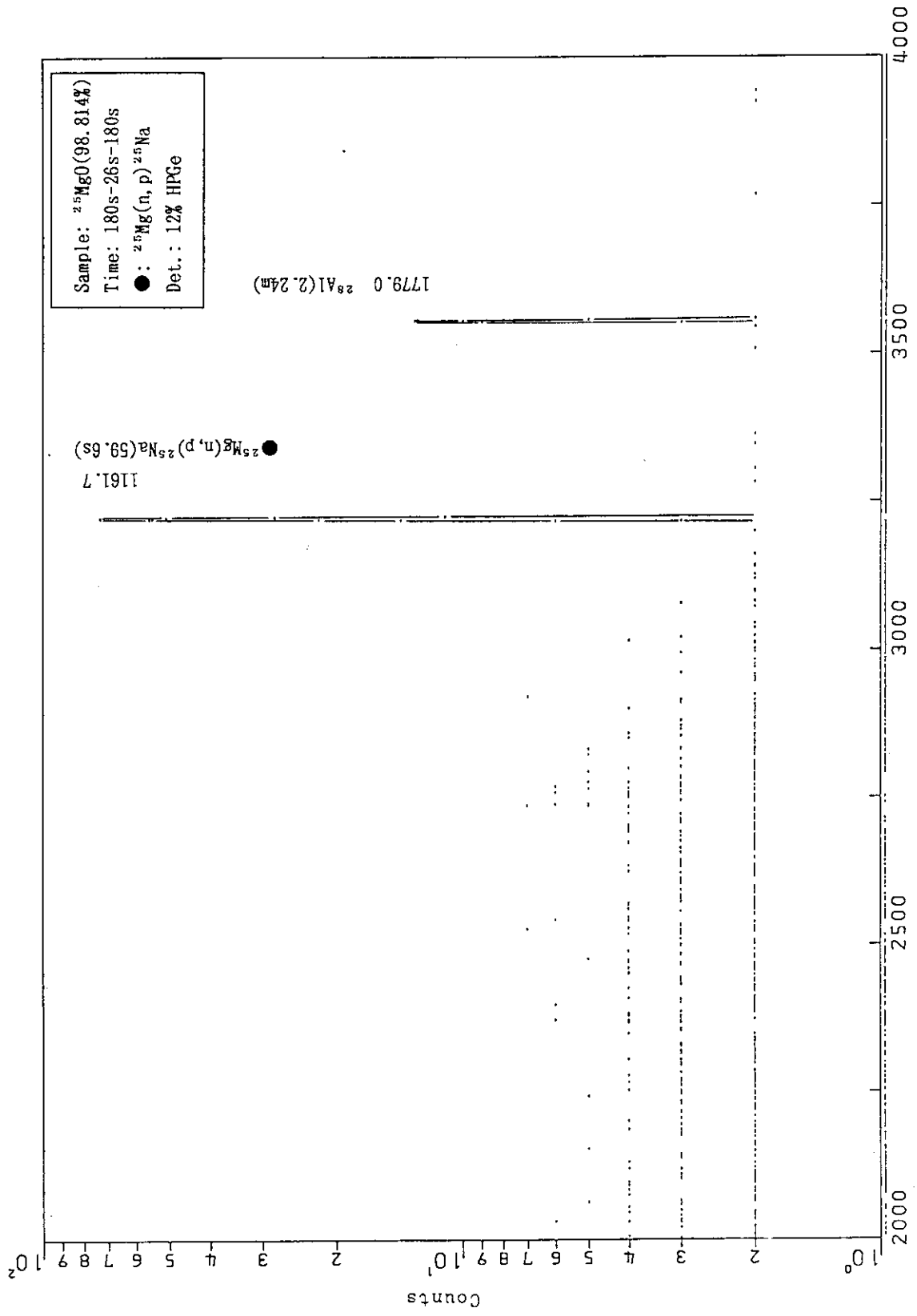
Sample: ^{25}MgO(98.814%)
Time: 180s-26s-180s
●: ^{25}Mg(n,p)^{25}Na
Det.: 12% HPGe
1779.0 ^{28}Al(2.24m)
●^{25}Mg(n,p)^{25}Na(59.6s)
1161.7
Counts
Channel Number

Fig. A.1.4

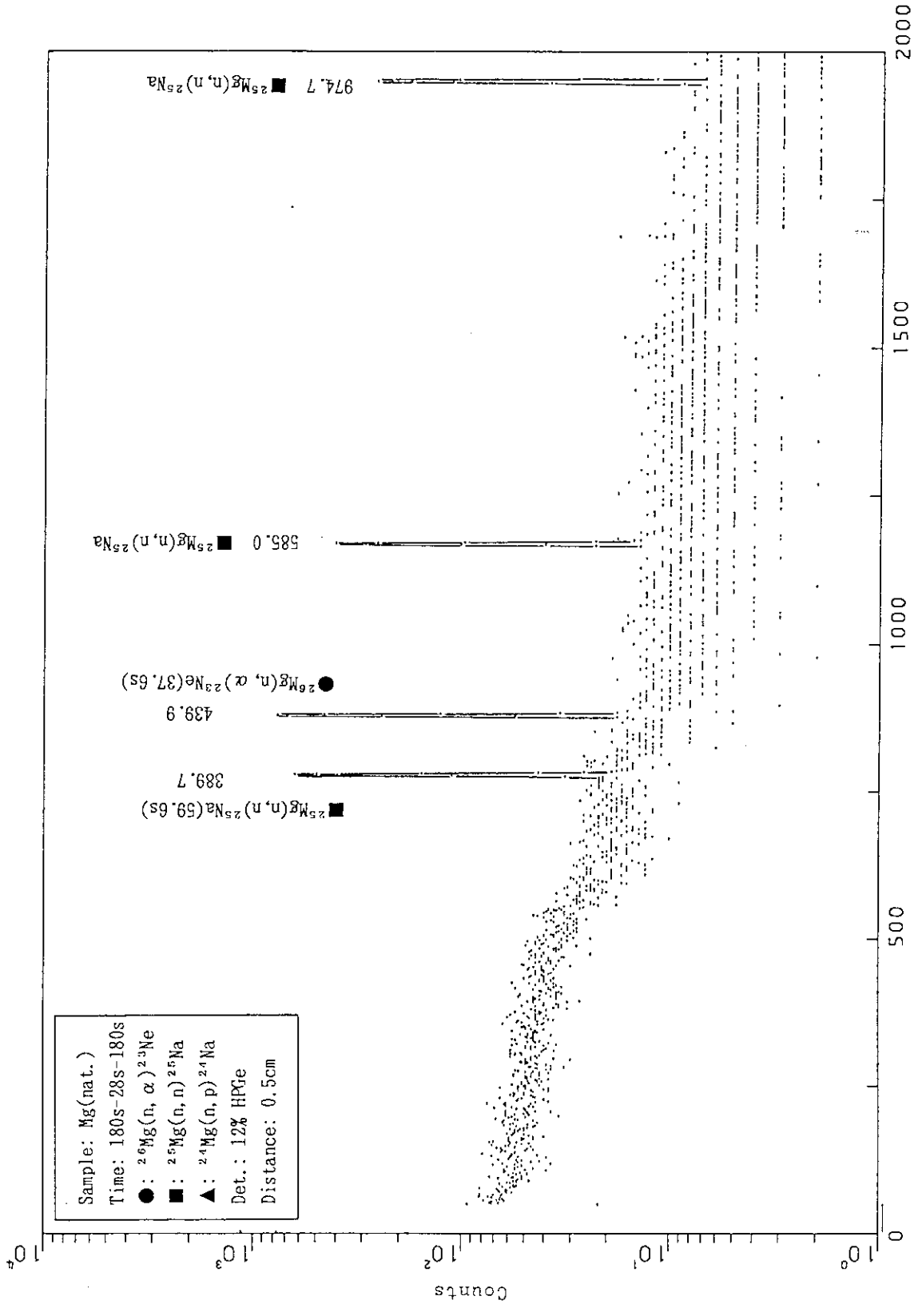
Sample: Mg(nat.)
Time: 180s-28s-180s
●: $^{26}Mg(n,\alpha)^{23}Ne$
■: $^{25}Mg(n,n)^{25}Na$
▲: $^{24}Mg(n,p)^{24}Na$
Det.: 12% HPGe
Distance: 0.5cm
■$^{25}Mg(n,n)^{25}Na$(59.6s)
389.7
439.9
●$^{26}Mg(n,\alpha)^{23}Ne$(37.6s)
585.0 ■$^{25}Mg(n,n)^{25}Na$
974.7 ■$^{25}Mg(n,n)^{25}Na$
Counts
Channel Number

Fig. A.1.5

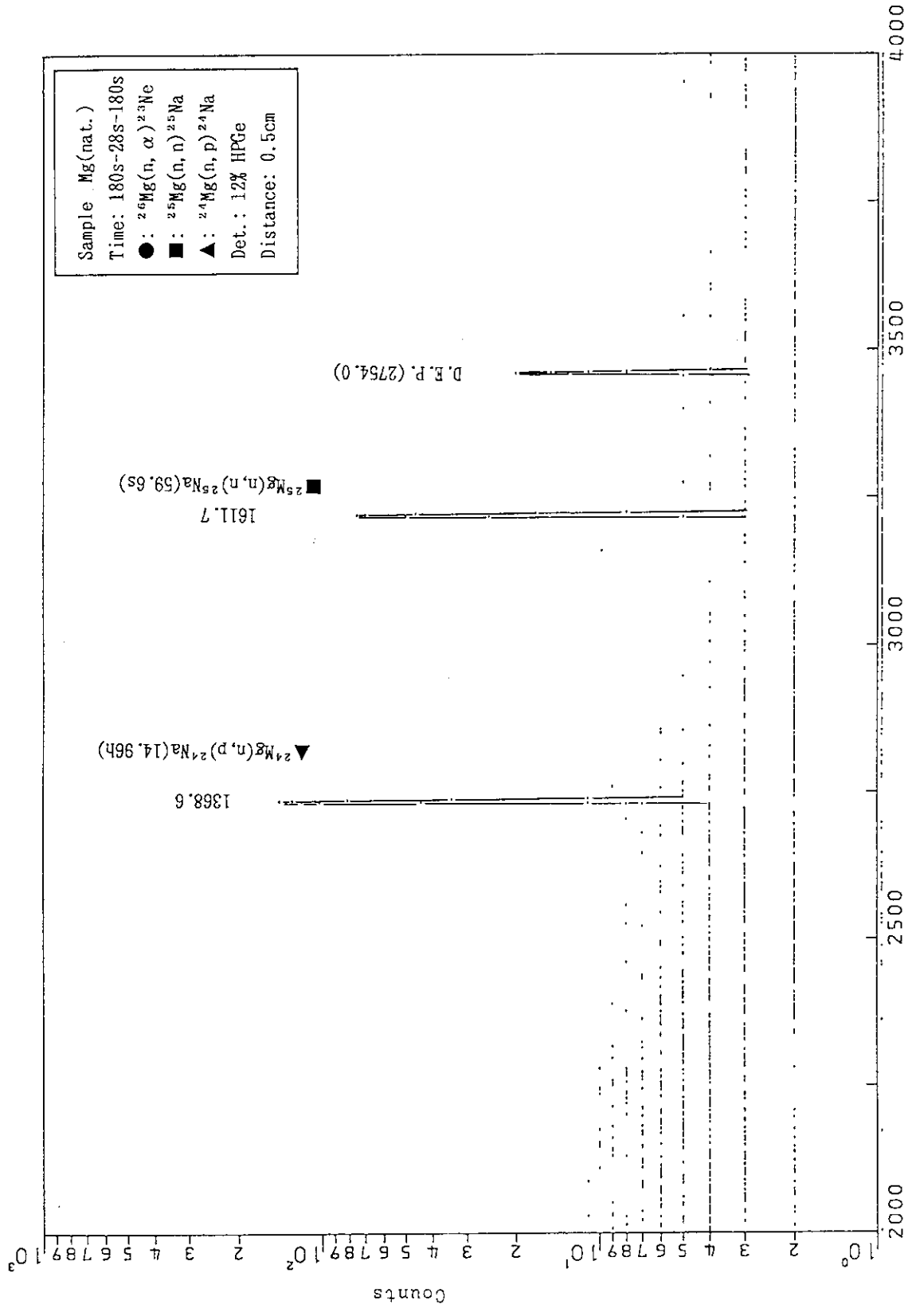
Sample Mg(nat.)
Time: 180s-28s-180s
●: $^{26}Mg(n,\alpha)^{23}Ne$
■: $^{25}Mg(n,n)^{25}Na$
▲: $^{24}Mg(n,p)^{24}Na$
Det.: 12% HPGe
Distance: 0.5cm
D.E.P.(2754.0)
■$^{25}Mg(n,n)^{25}Na(59.6s)$
1611.7
▲$^{24}Mg(n,p)^{24}Na(14.96h)$
1368.6
Counts
Channel Number

Fig. A.1.6

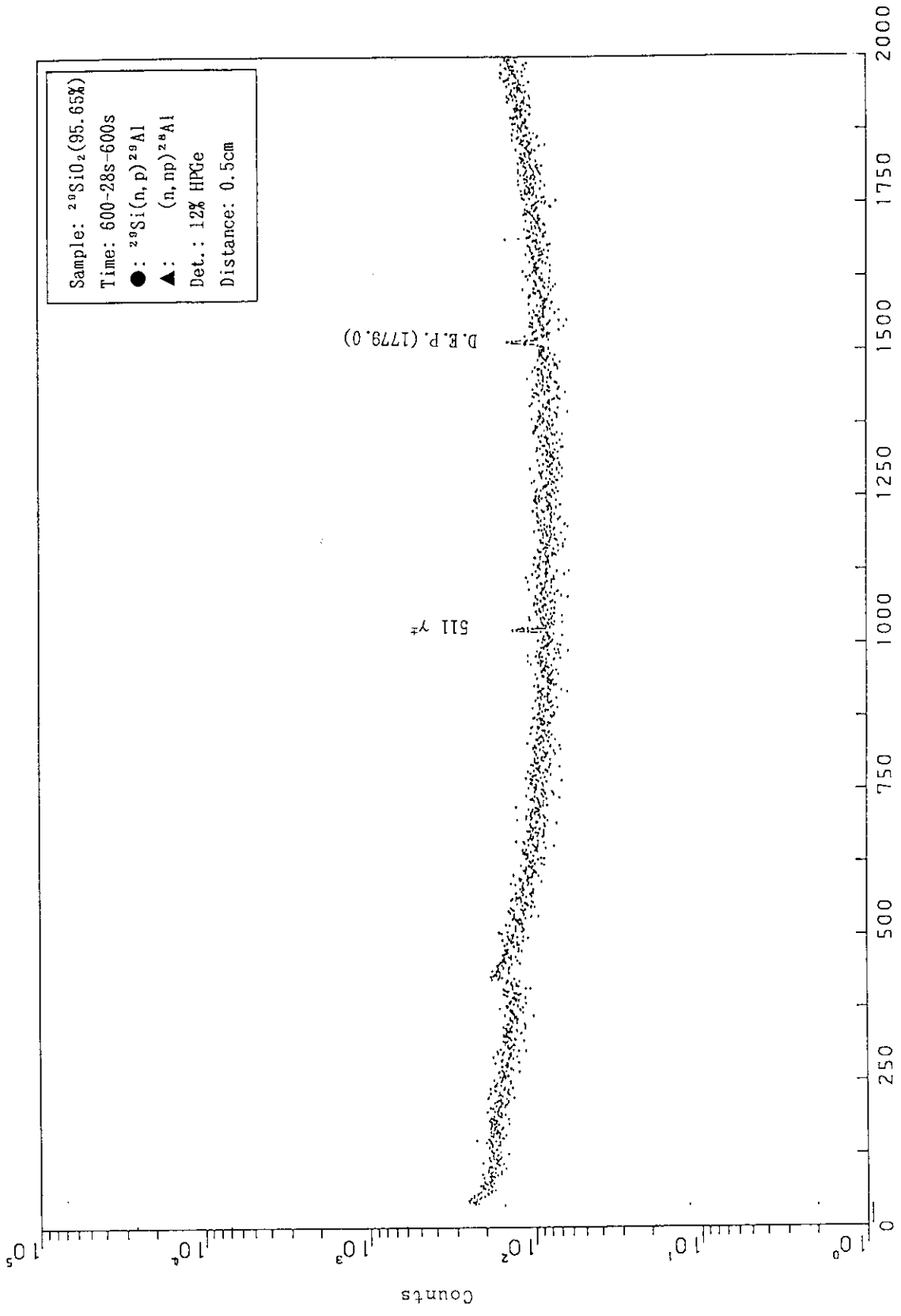
Sample: $^{29}SiO_2$(95.65%)
Time: 600-28s-600s
●: $^{29}Si(n,p)^{29}Al$
▲: $(n,np)^{28}Al$
Det.: 12% HPGe
Distance: 0.5cm
D.E.P.(1779.0)
511 γ
Counts
Channel Number
0
250
500
750
1000
1250
1500
1750
2000

Fig. A.1.7

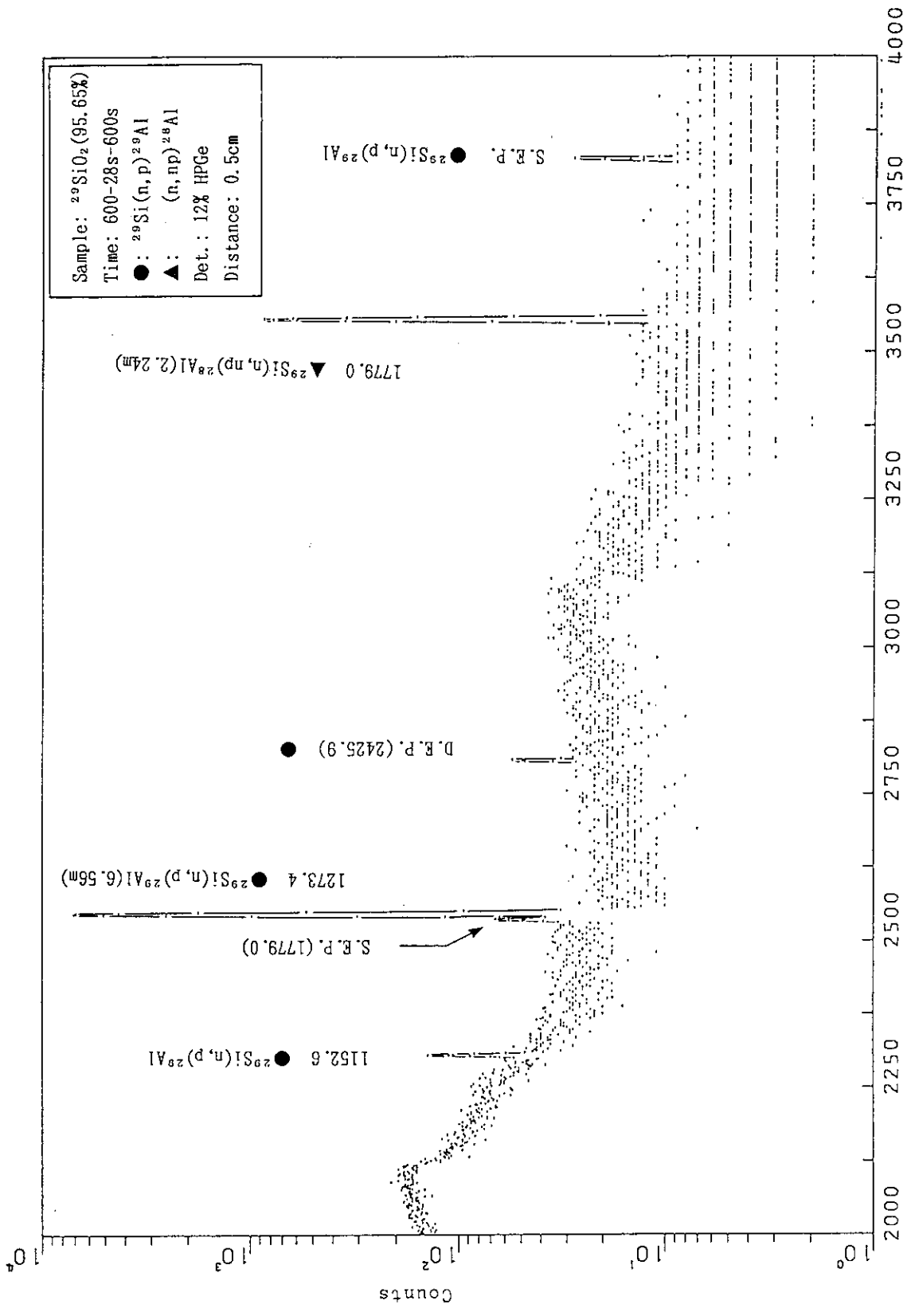
Sample: $^{29}SiO_2$(95.65%)
Time: 600-28s-600s
●: $^{29}Si(n,p)^{29}Al$
▲: $(n,np)^{28}Al$
Det.: 12% HPGe
Distance: 0.5cm
S.E.P. ●$^{29}Si(n,p)^{29}Al$
1779.0 ▲$^{29}Si(n,np)^{28}Al$(2.24m)
D.E.P.(2425.9) ●
1273.4 ●$^{29}Si(n,p)^{29}Al$(6.56m)
S.E.P.(1779.0)
1152.6 ●$^{29}Si(n,p)^{29}Al$
Counts
Channel Number

Fig. A.1.8

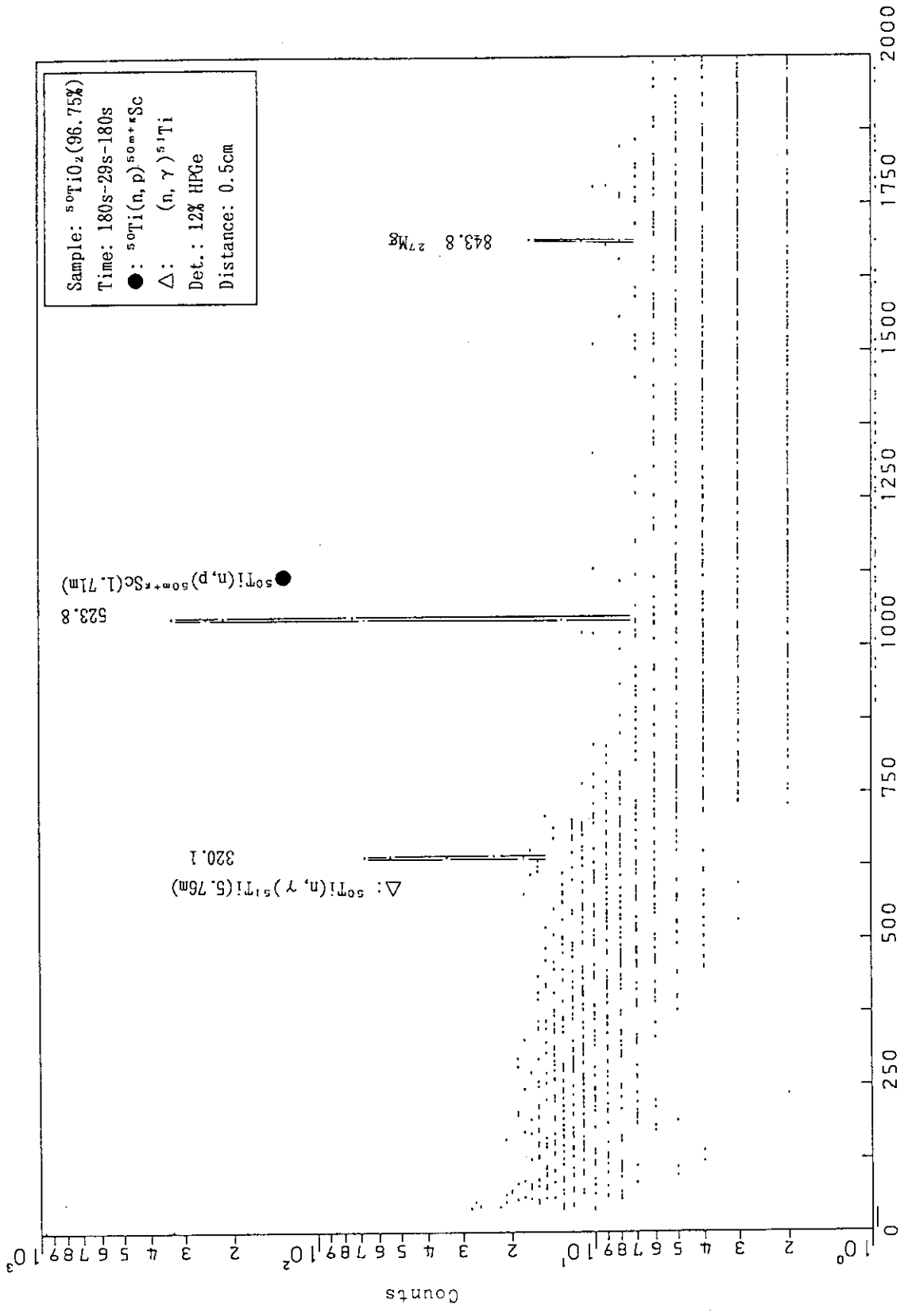
Sample: $^{50}TiO_2$(96.75%)
Time: 180s-29s-180s
●: $^{50}Ti(n,p)^{50m+g}Sc$
△: $(n,\gamma)^{51}Ti$
Det.: 12% HPGe
Distance: 0.5cm
843.8 ^{27}Mg
●$^{50}Ti(n,p)^{50m+g}Sc(1.71m)$
523.8
△: $^{50}Ti(n,\gamma)^{51}Ti(5.76m)$
320.1
Counts
Channel Number
0
250
500
750
1000
1250
1500
1750
2000

Fig. A.1.9

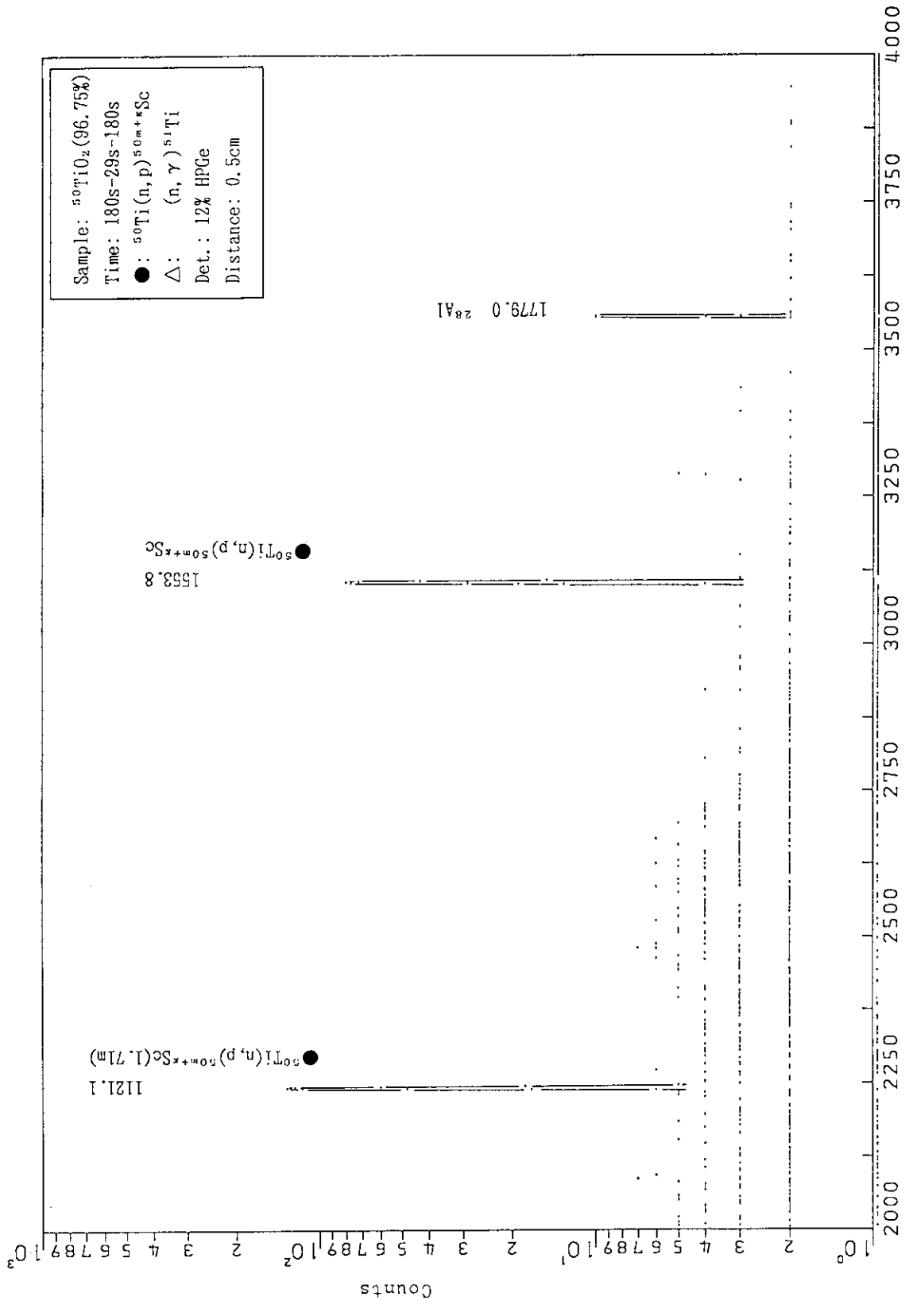
Sample: $^{50}TiO_2$(96.75%)
Time: 180s-29s-180s
●: $^{50}Ti(n,p)^{50m+g}Sc$
△: $(n,\gamma)^{51}Ti$
Det.: 12% HPGe
Distance: 0.5cm
1779.0 ^{28}Al
1553.8
●$^{50}Ti(n,p)^{50m+g}Sc$
1121.1
●$^{50}Ti(n,p)^{50m+g}Sc(1.71m)$
Counts
Channel Number

Fig. A.1.10

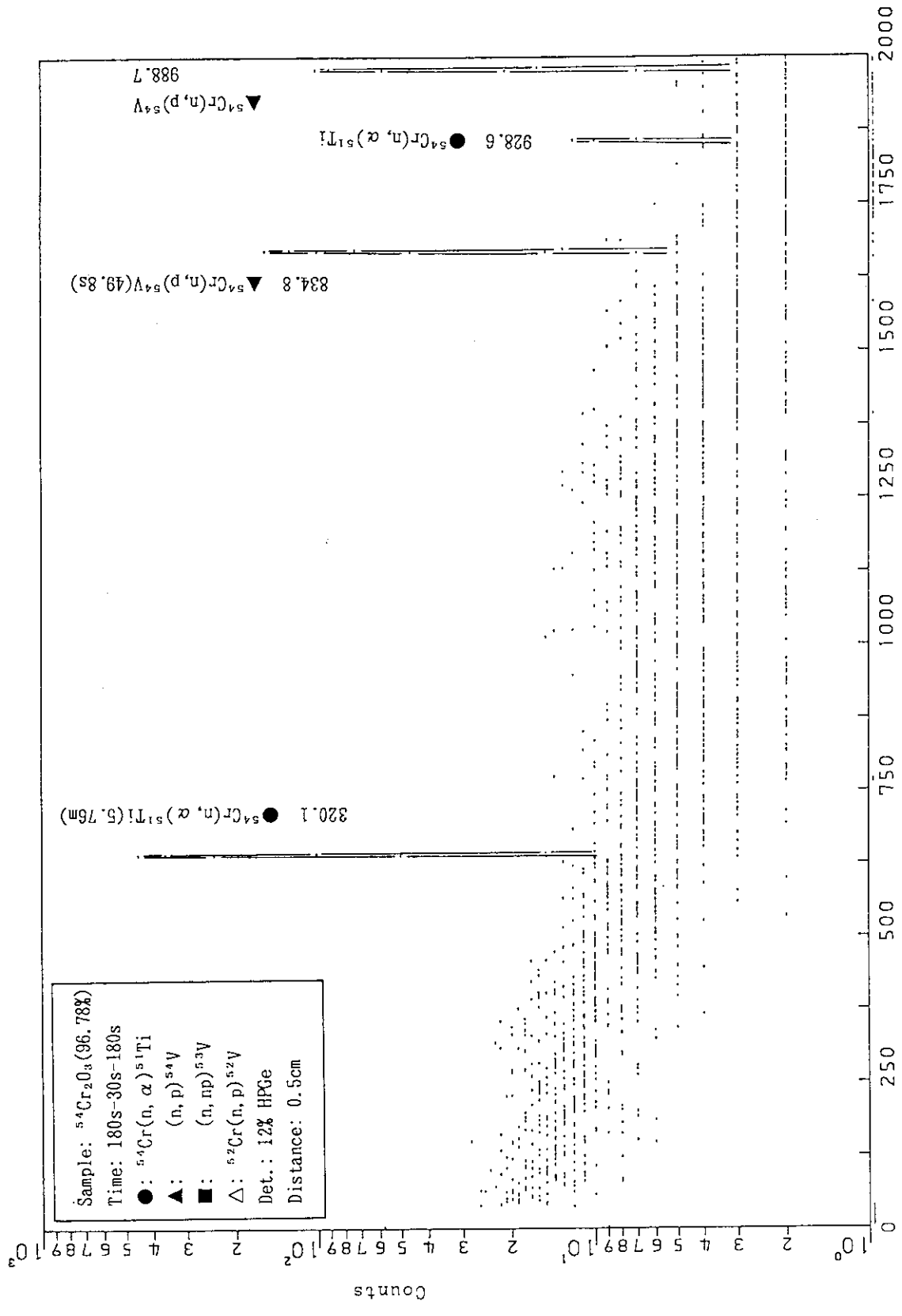
Sample: $^{54}Cr_2O_3$(96.78%)
Time: 180s-30s-180s
●: $^{54}Cr(n,\alpha)^{51}Ti$
▲: $(n,p)^{54}V$
■: $(n,np)^{53}V$
△: $^{52}Cr(n,p)^{52}V$
Det.: 12% HPGe
Distance: 0.5cm
320.1 ●$^{54}Cr(n,\alpha)^{51}Ti$(5.76m)
834.8 ▲$^{54}Cr(n,p)^{54}V$(49.8s)
928.6 ●$^{54}Cr(n,\alpha)^{51}Ti$
▲$^{54}Cr(n,p)^{54}V$
988.7
Counts
Channel Number

Fig. A.1.11

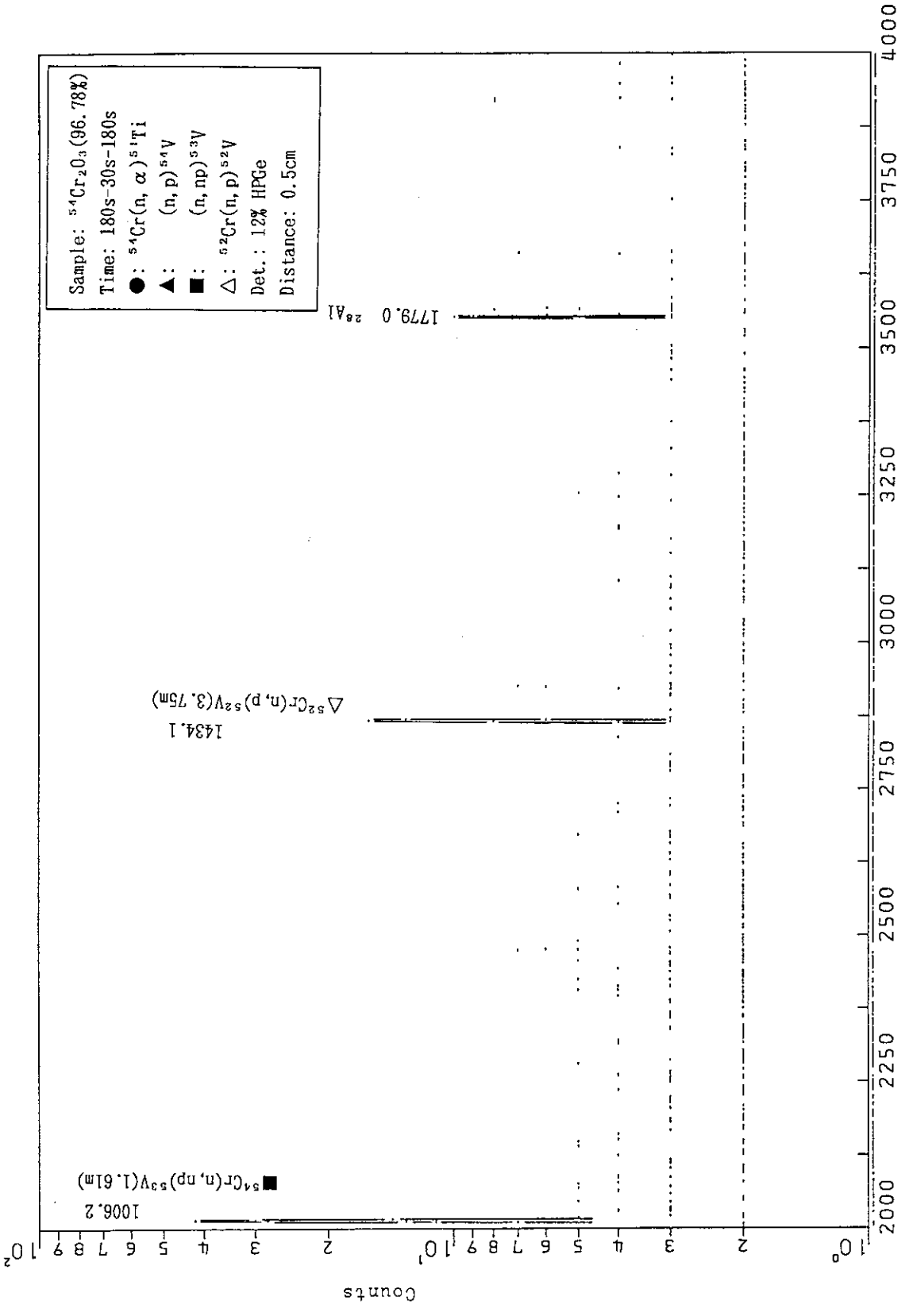
Sample: $^{54}Cr_2O_3$(96.78%)
Time: 180s-30s-180s
●: $^{54}Cr(n,\alpha)^{51}Ti$
▲: $(n,p)^{54}V$
■: $(n,np)^{53}V$
△: $^{52}Cr(n,p)^{52}V$
Det.: 12% HPGe
Distance: 0.5cm
1779.0 ^{28}Al
1434.1
$\triangle^{52}Cr(n,p)^{52}V(3.75m)$
1006.2
■$^{54}Cr(n,np)^{53}V(1.61m)$
Counts
Channel Number

Fig. A.1.12

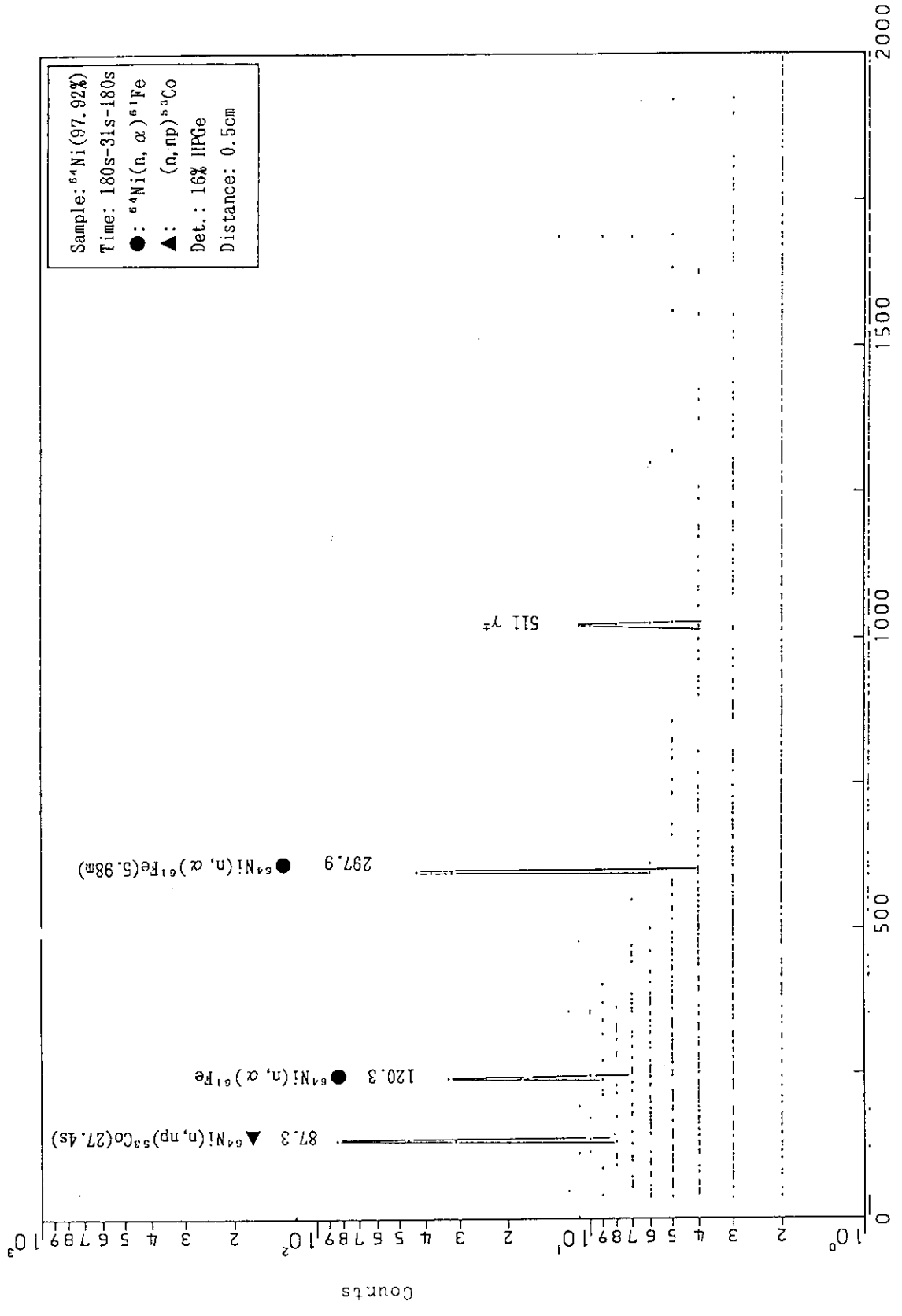
Sample: ^{64}Ni(97.92%)
Time: 180s-31s-180s
●: ^{64}Ni(n, α)^{61}Fe
▲: (n, np)^{53}Co
Det.: 16% HPGe
Distance: 0.5cm
87.3 ▲^{64}Ni(n,np)^{53}Co(27.4s)
120.3 ●^{64}Ni(n, α)^{61}Fe
297.9 ●^{64}Ni(n, α)^{61}Fe(5.98m)
511 γ±
Counts
Channel Number
0
500
1000
1500
2000

Fig. A.1.13

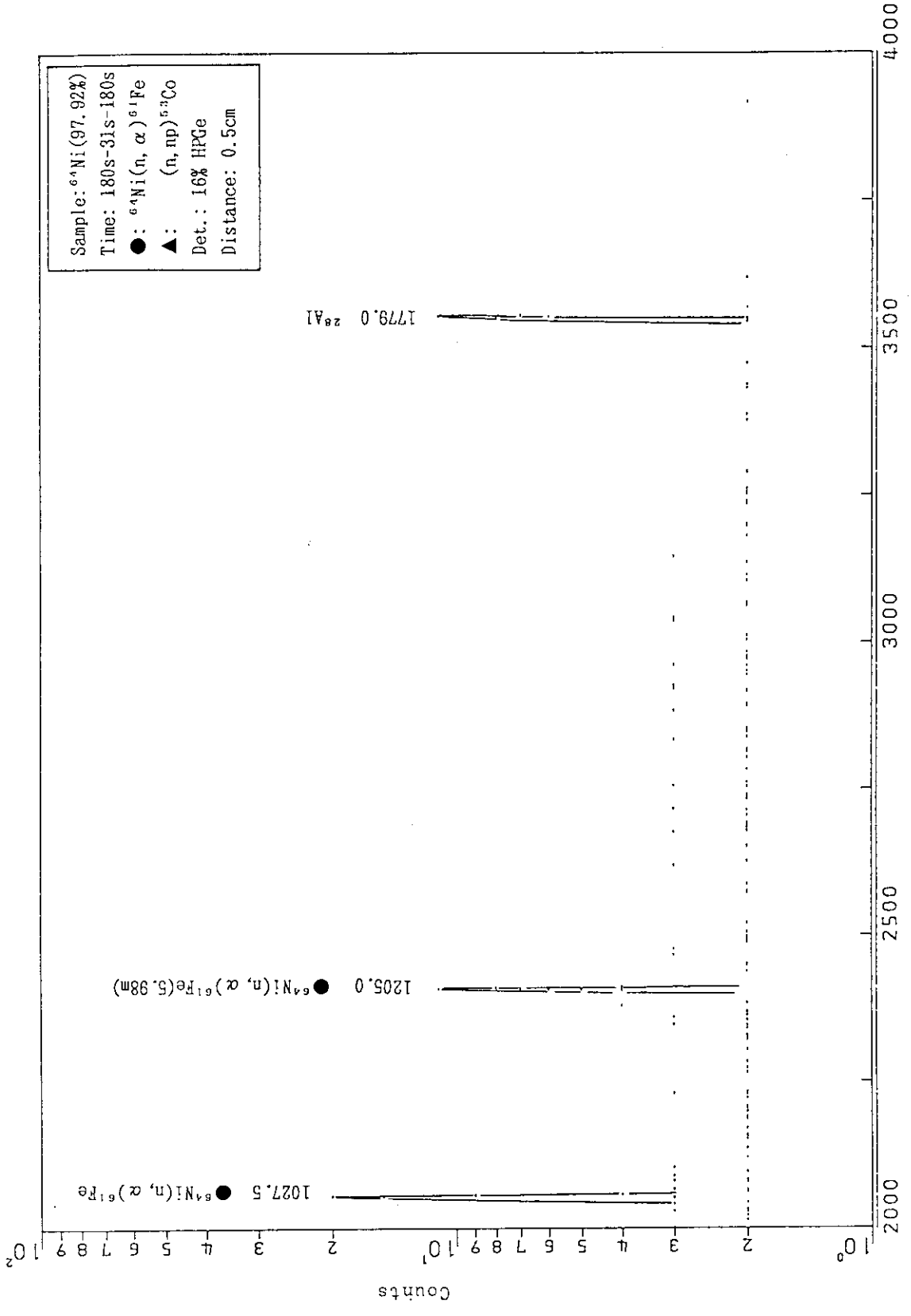
Sample: ^{64}Ni(97.92%)
Time: 180s-31s-180s
●: ^{64}Ni(n, α)^{61}Fe
▲: (n, np)^{63}Co
Det.: 16% HPGe
Distance: 0.5cm
1779.0 ^{28}Al
1205.0 ●^{64}Ni(n, α)^{61}Fe(5.98m)
1027.5 ●^{64}Ni(n, α)^{61}Fe
Counts
Channel Number

Fig. A.1.14

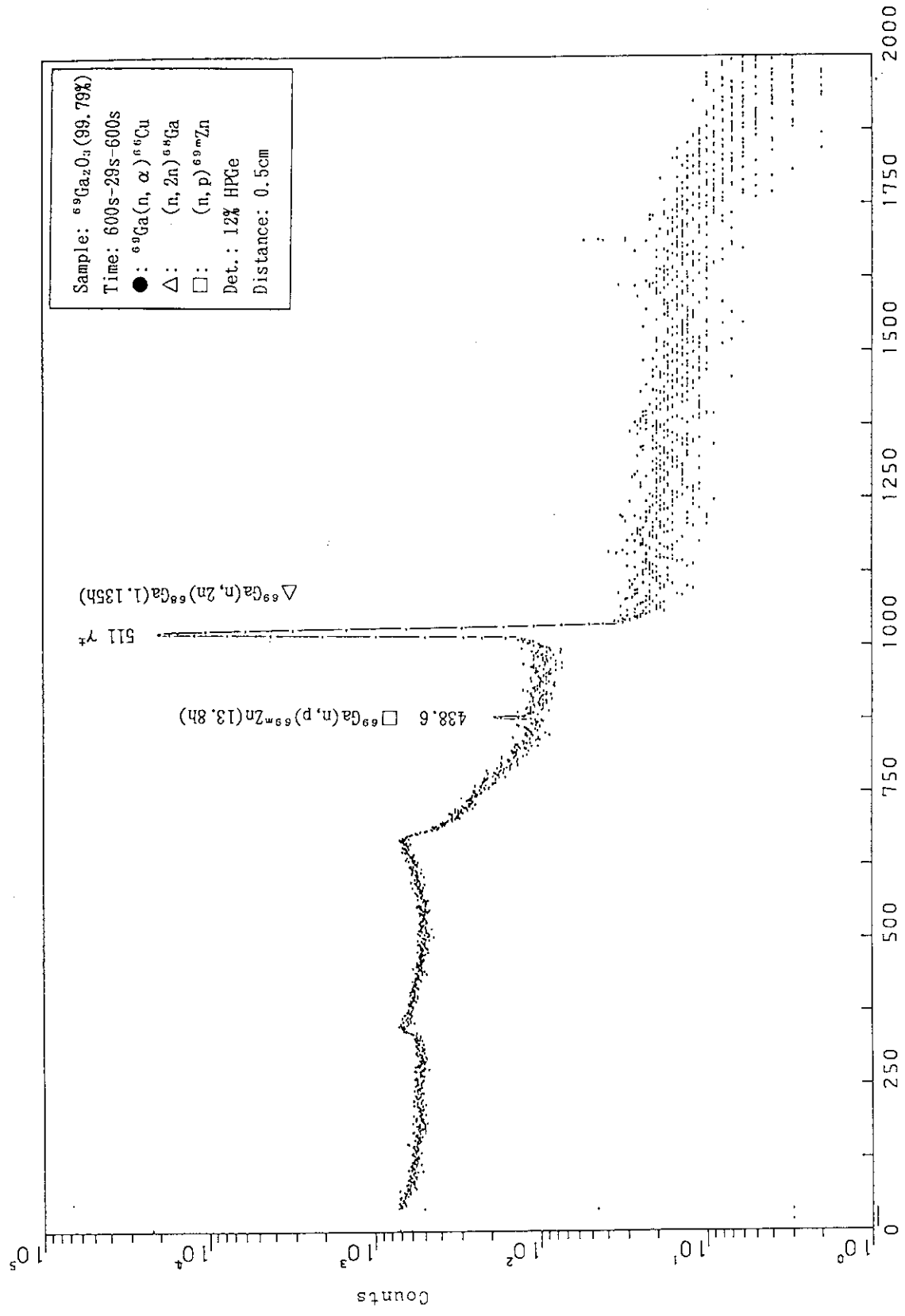
Sample: $^{69}Ga_2O_3$(99.79%)
Time: 600s-29s-600s
●: $^{69}Ga(n,\alpha)^{66}Cu$
△: $(n,2n)^{68}Ga$
□: $(n,p)^{69m}Zn$
Det.: 12% HPGe
Distance: 0.5cm
△$^{69}Ga(n,2n)^{68}Ga(1.135h)$
511 γ*
438.6 □$^{69}Ga(n,p)^{69m}Zn(13.8h)$
Counts
Channel Number

Fig. A.1.15

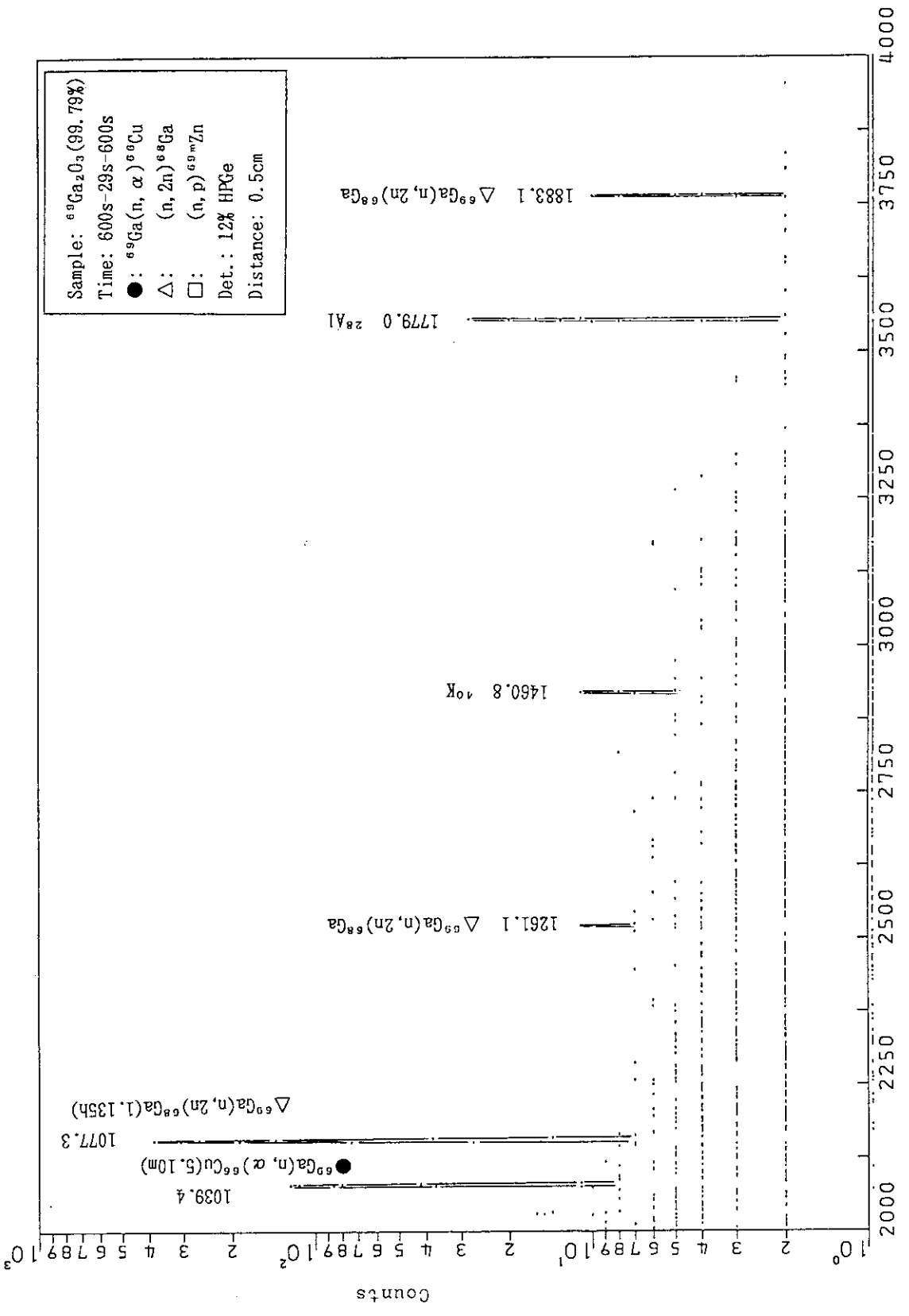
Sample: $^{69}Ga_2O_3$(99.79%)
Time: 600s-29s-600s
●: $^{69}Ga(n,\alpha)^{66}Cu$
△: $(n,2n)^{68}Ga$
□: $(n,p)^{69m}Zn$
Det.: 12% HPGe
Distance: 0.5cm
1883.1 △$^{69}Ga(n,2n)^{68}Ga$
1779.0 ^{28}Al
1460.8 ^{40}K
1261.1 △$^{69}Ga(n,2n)^{68}Ga$
1039.4
●$^{69}Ga(n,\alpha)^{66}Cu(5.10m)$
1077.3
△$^{69}Ga(n,2n)^{68}Ga(1.135h)$
Counts
Channel Number

Fig. A.1.16

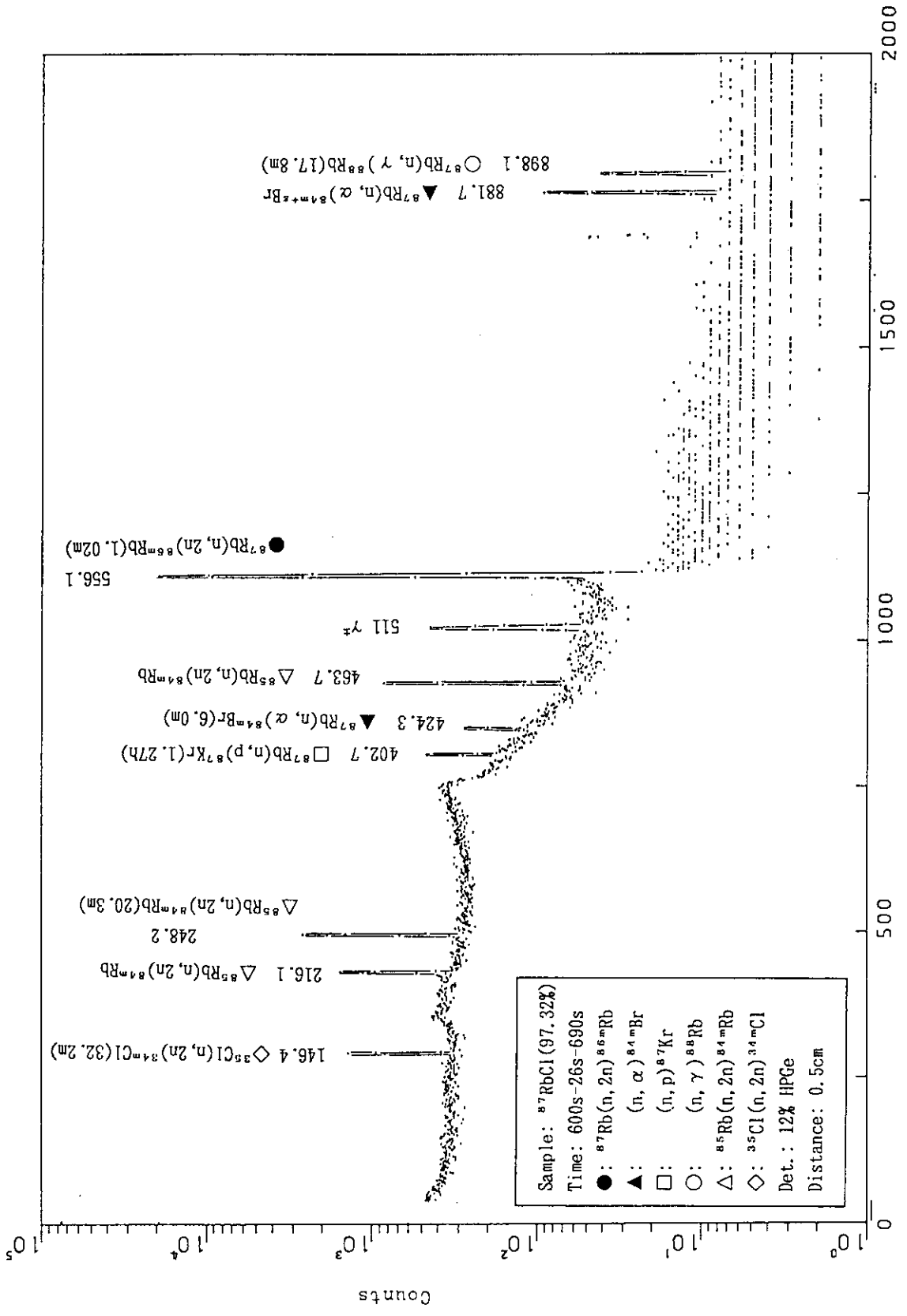
Sample: ^{87}RbCl(97.32%)
Time: 600s-26s-690s
●: ^{87}Rb(n,2n)^{86m}Rb
▲: (n,α)^{84m}Br
□: (n,p)^{87}Kr
○: (n,γ)^{88}Rb
△: ^{85}Rb(n,2n)^{84m}Rb
◇: ^{35}Cl(n,2n)^{34m}Cl
Det.: 12% HPGe
Distance: 0.5cm
146.4 ◇^{35}Cl(n,2n)^{34m}Cl(32.2m)
216.1 △^{85}Rb(n,2n)^{84m}Rb
248.2
△^{85}Rb(n,2n)^{84m}Rb(20.3m)
402.7 □^{87}Rb(n,p)^{87}Kr(1.27h)
424.3 ▲^{87}Rb(n,α)^{84m}Br(6.0m)
463.7 △^{85}Rb(n,2n)^{84m}Rb
511 γ*
556.1
●^{87}Rb(n,2n)^{86m}Rb(1.02m)
881.7 ▲^{87}Rb(n,α)$^{84m+g}$Br
898.1 ○^{87}Rb(n,γ)^{88}Rb(17.8m)
Counts
Channel Number
0
500
1000
1500
2000

Fig. A.1.17

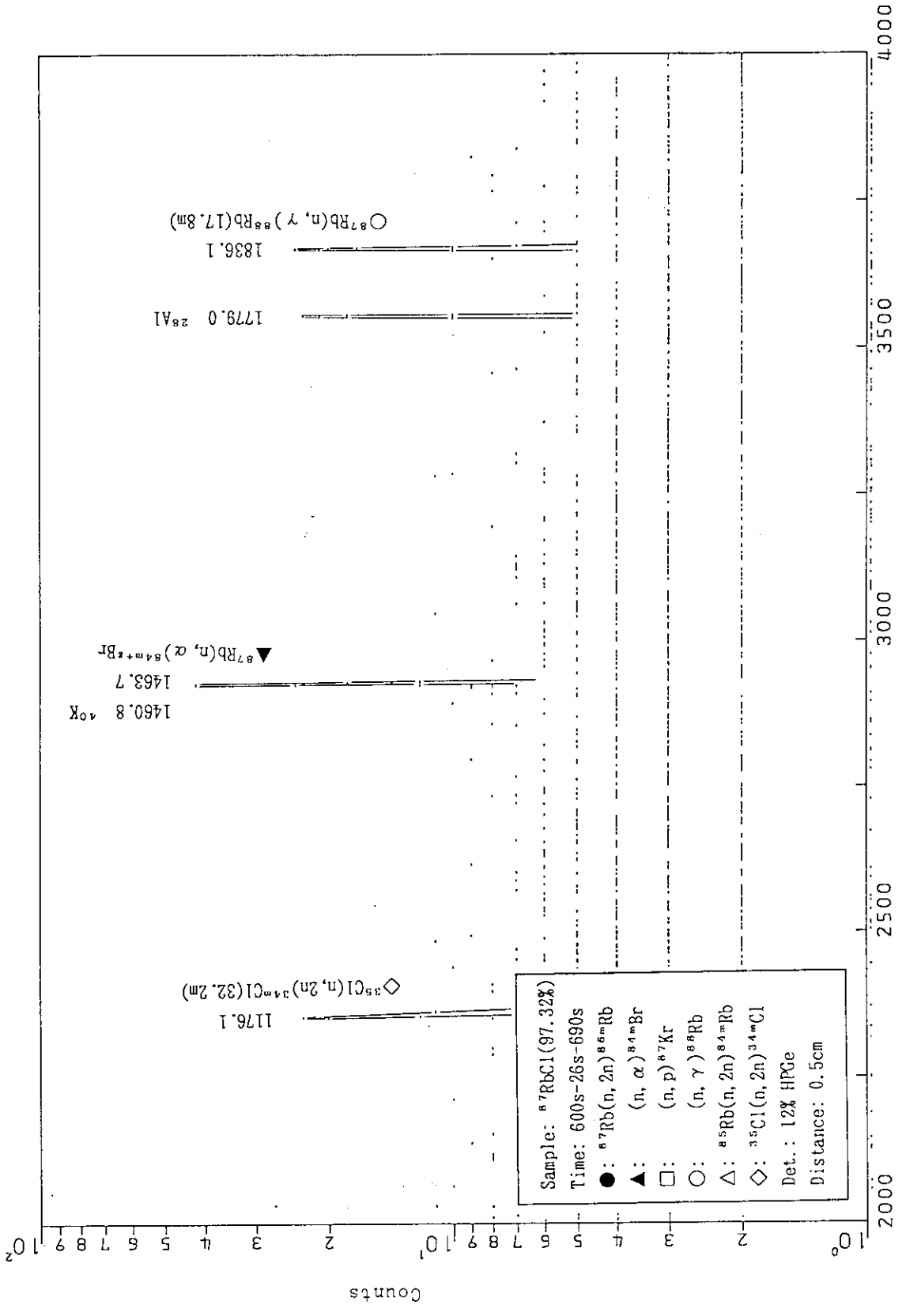
Sample: $^{87}RbCl$(97.32%)
Time: 600s-26s-690s
●: $^{87}Rb(n,2n)^{86m}Rb$
▲: $(n,\alpha)^{84m}Br$
□: $(n,p)^{87}Kr$
○: $(n,\gamma)^{88}Rb$
△: $^{85}Rb(n,2n)^{84m}Rb$
◇: $^{35}Cl(n,2n)^{34m}Cl$
Det.: 12% HPGe
Distance: 0.5cm
◇$^{35}Cl(n,2n)^{34m}Cl$(32.2m)
1176.1
▲$^{87}Rb(n,\alpha)^{84m+g}Br$
1460.8 ^{40}K
1463.7
1779.0 ^{28}Al
○$^{87}Rb(n,\gamma)^{88}Rb$(17.8m)
1836.1
Counts
Channel Number

Fig. A.1.18

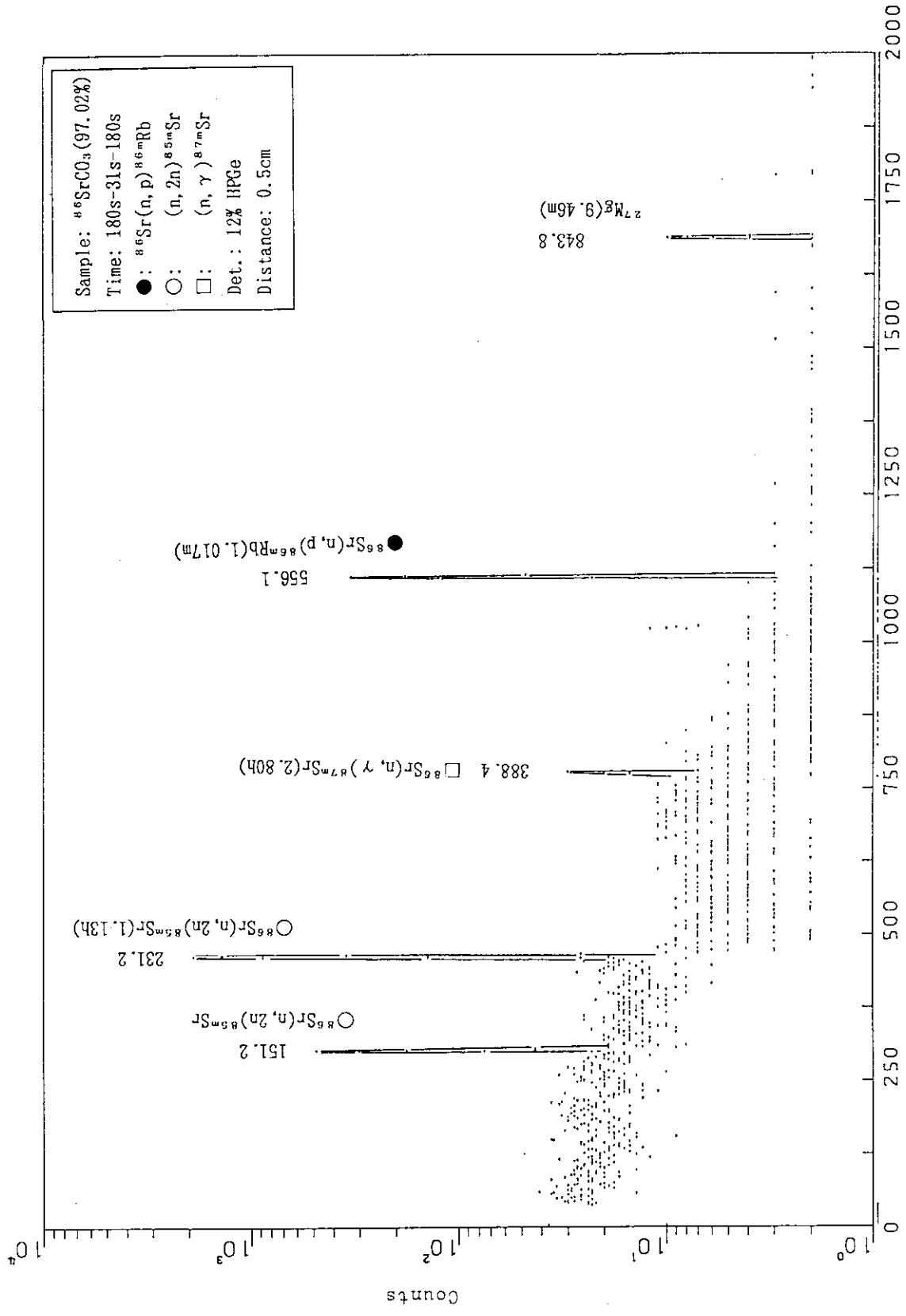
Sample: $^{86}SrCO_3$(97.02%)
Time: 180s-31s-180s
●: $^{86}Sr(n,p)^{86m}Rb$
○: $(n,2n)^{85m}Sr$
□: $(n,\gamma)^{87m}Sr$
Det.: 12% HPGe
Distance: 0.5cm
843.8
^{27}Mg(9.46m)
556.1
●$^{86}Sr(n,p)^{86m}Rb$(1.017m)
388.4 □$^{86}Sr(n,\gamma)^{87m}Sr$(2.80h)
231.2
○$^{86}Sr(n,2n)^{85m}Sr$(1.13h)
151.2
○$^{86}Sr(n,2n)^{85m}Sr$
Counts
Channel Number

Fig. A.1.19

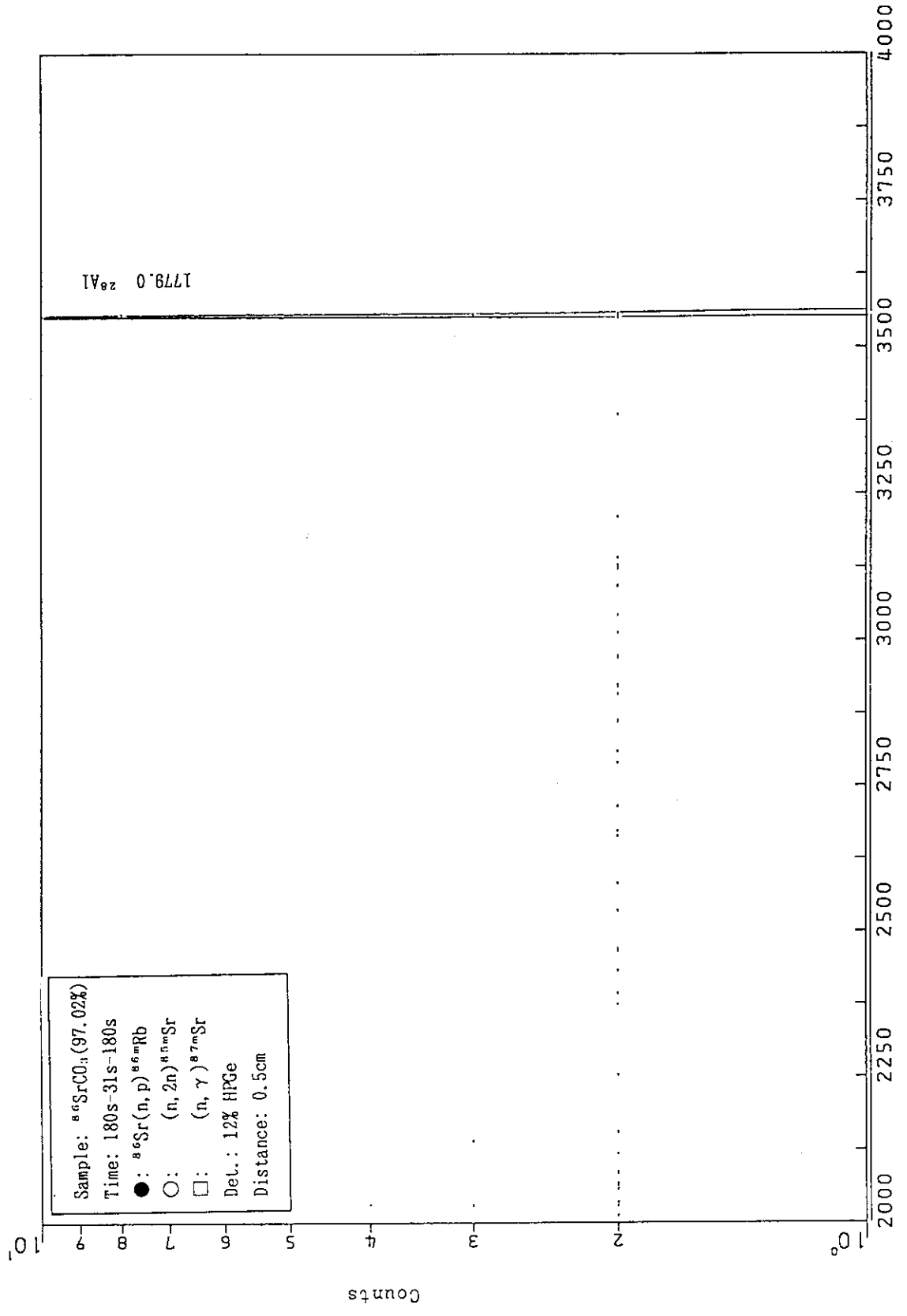
Sample: $^{86}SrCO_3$(97.02%)
Time: 180s-31s-180s
●: $^{86}Sr(n,p)^{86m}Rb$
○: $(n,2n)^{85m}Sr$
□: $(n,\gamma)^{87m}Sr$
Del.: 12% HPGe
Distance: 0.5cm
1779.0 keV ^{28}Al
Counts
Channel Number
10^0
10^1
2000
2250
2500
2750
3000
3250
3500
3750
4000

Fig. A.1.20

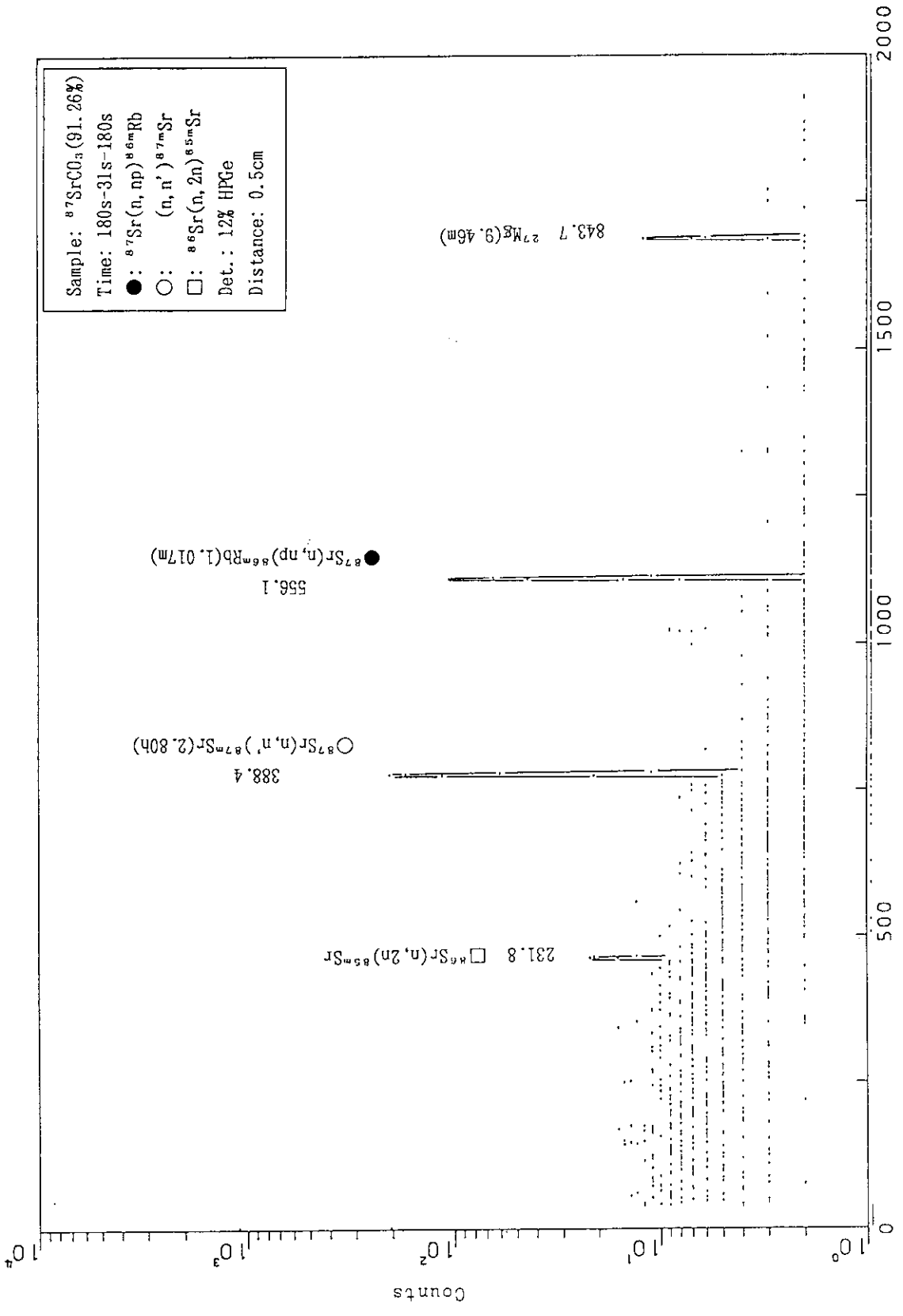
Sample: $^{87}SrCO_3$(91.26%)
Time: 180s-31s-180s
●: $^{87}Sr(n,np)^{86m}Rb$
○: $(n,n')^{87m}Sr$
□: $^{86}Sr(n,2n)^{85m}Sr$
Det.: 12% HPGe
Distance: 0.5cm
231.8 □$^{86}Sr(n,2n)^{85m}Sr$
388.4
○$^{87}Sr(n,n')^{87m}Sr$(2.80h)
556.1
●$^{87}Sr(n,np)^{86m}Rb$(1.017m)
843.7 ^{27}Mg(9.46m)
Counts
Channel Number

Fig. A.1.21

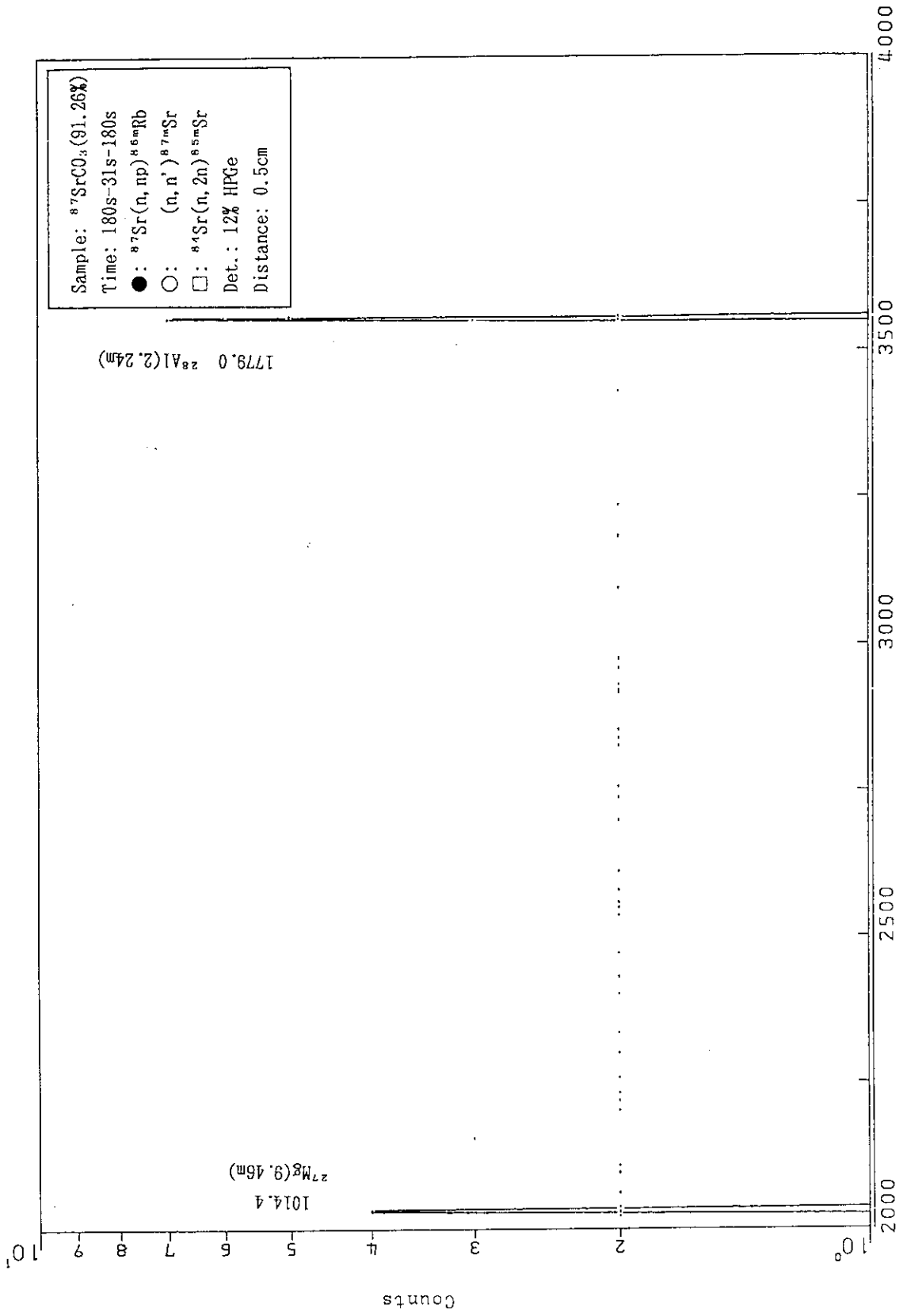
Sample: $^{87}SrCO_3$(91.26%)
Time: 180s-31s-180s
●: $^{87}Sr(n,np)^{86m}Rb$
○: $(n,n')^{87m}Sr$
□: $^{84}Sr(n,2n)^{85m}Sr$
Det.: 12% HPGe
Distance: 0.5cm
1779.0 ^{28}Al(2.24m)
1014.4
^{27m}Mg(9.46m)
Counts
Channel Number

Fig. A.1.22

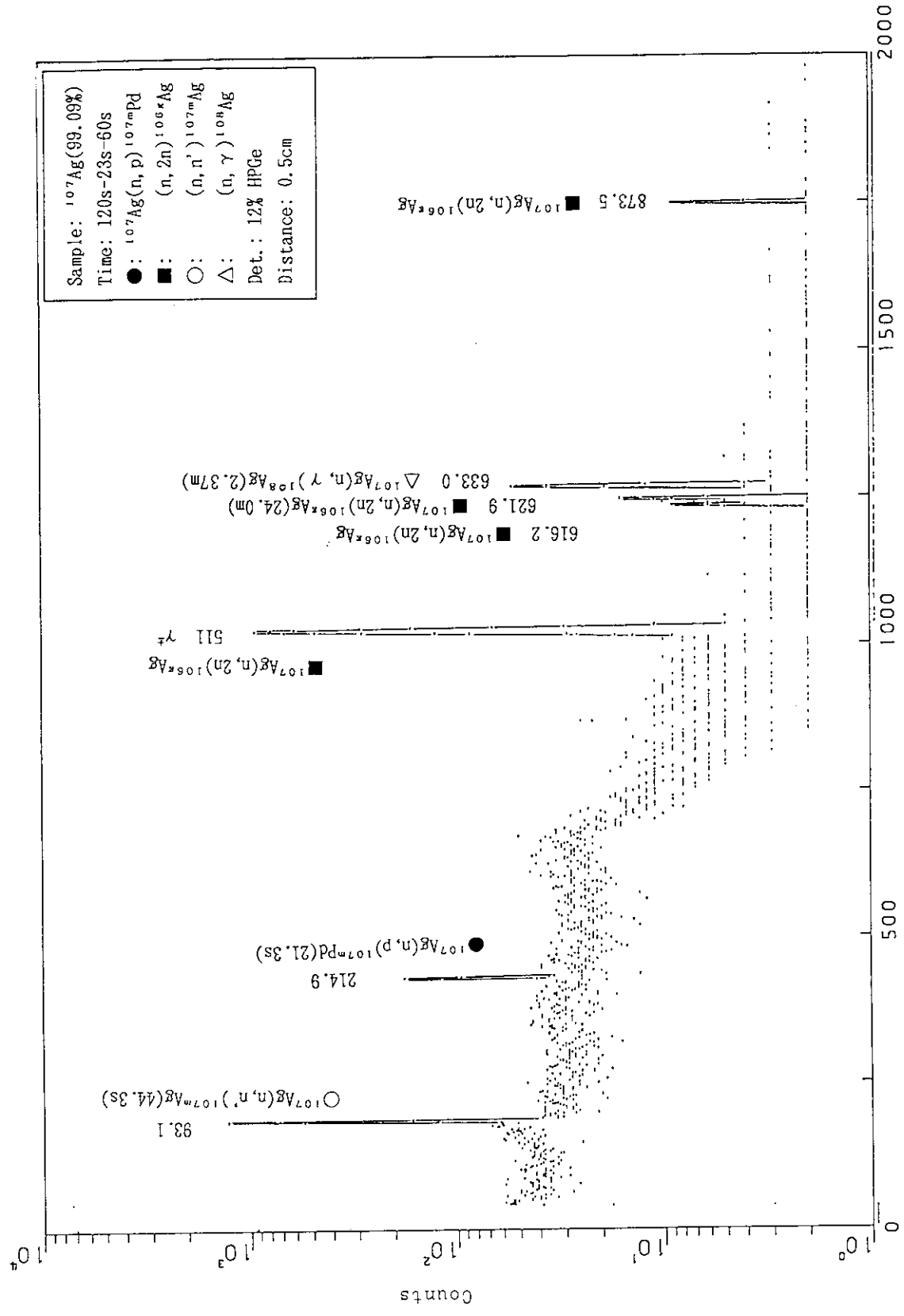
Sample: ^{107}Ag(99.09%)
Time: 120s-23s-60s
●: ^{107}Ag(n,p)^{107m}Pd
■: (n,2n)$^{106\kappa}$Ag
○: (n,n')^{107m}Ag
△: (n,γ)^{108}Ag
Det.: 12% HPGe
Distance: 0.5cm
873.5 ■^{107}Ag(n,2n)$^{106\kappa}$Ag
633.0 △^{107}Ag(n,γ)^{108}Ag(2.37m)
621.9 ■^{107}Ag(n,2n)$^{106\kappa}$Ag(24.0m)
616.2 ■^{107}Ag(n,2n)$^{106\kappa}$Ag
511 γ±
■^{107}Ag(n,2n)$^{106\kappa}$Ag
214.9
●^{107}Ag(n,p)^{107m}Pd(21.3s)
93.1
○^{107}Ag(n,n')^{107m}Ag(44.3s)
Counts
Channel Number

Fig. A.1.23

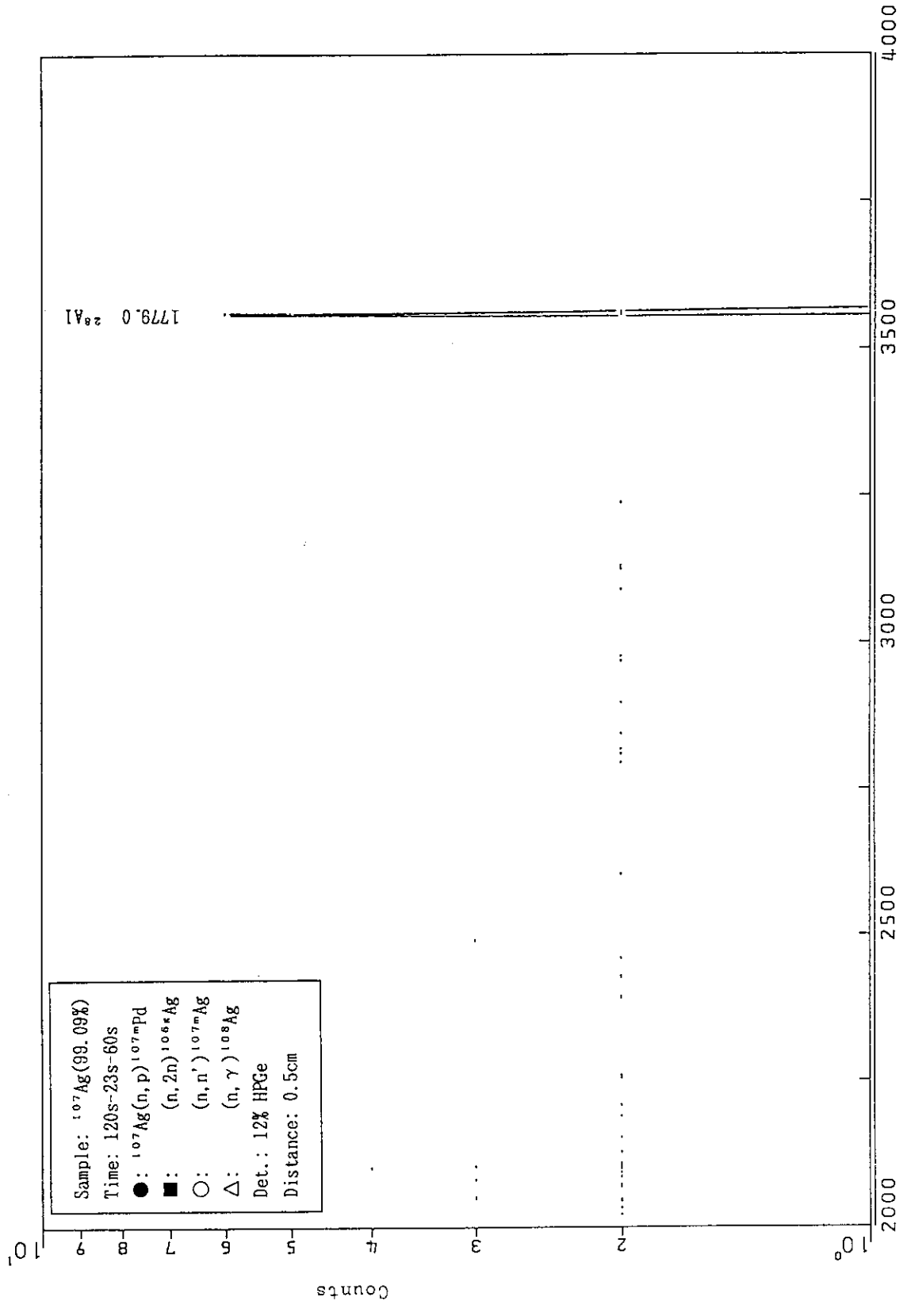
Sample: ^{107}Ag(99.09%)
Time: 120s-23s-60s
●: ^{107}Ag(n,p)^{107m}Pd
■: (n,2n)^{106g}Ag
○: (n,n')^{107m}Ag
△: (n,γ)^{108}Ag
Det.: 12% HPGe
Distance: 0.5cm
1779.0 ^{28}Al
Counts
Channel Number

Fig. A.1.24

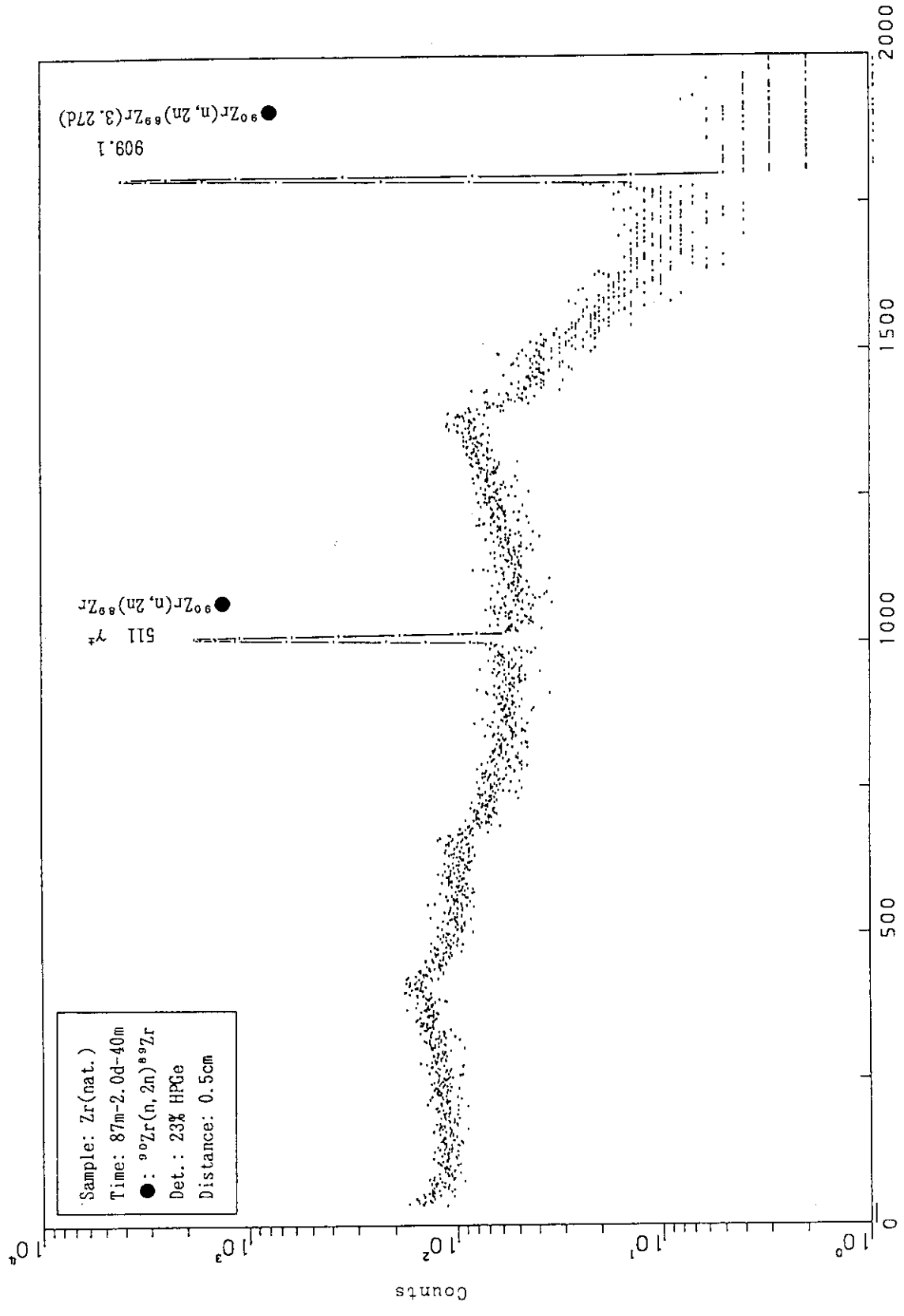
Sample: Zr(nat.)
Time: 87m-2.0d-40m
●: $^{90}Zr(n,2n)^{89}Zr$
Det.: 23% HPGe
Distance: 0.5cm
$^{90}Zr(n,2n)^{89}Zr$
511 γ±
$^{90}Zr(n,2n)^{89}Zr(3.27d)$
909.1
Counts
Channel Number
0
500
1000
1500
2000

Fig. A.1.25

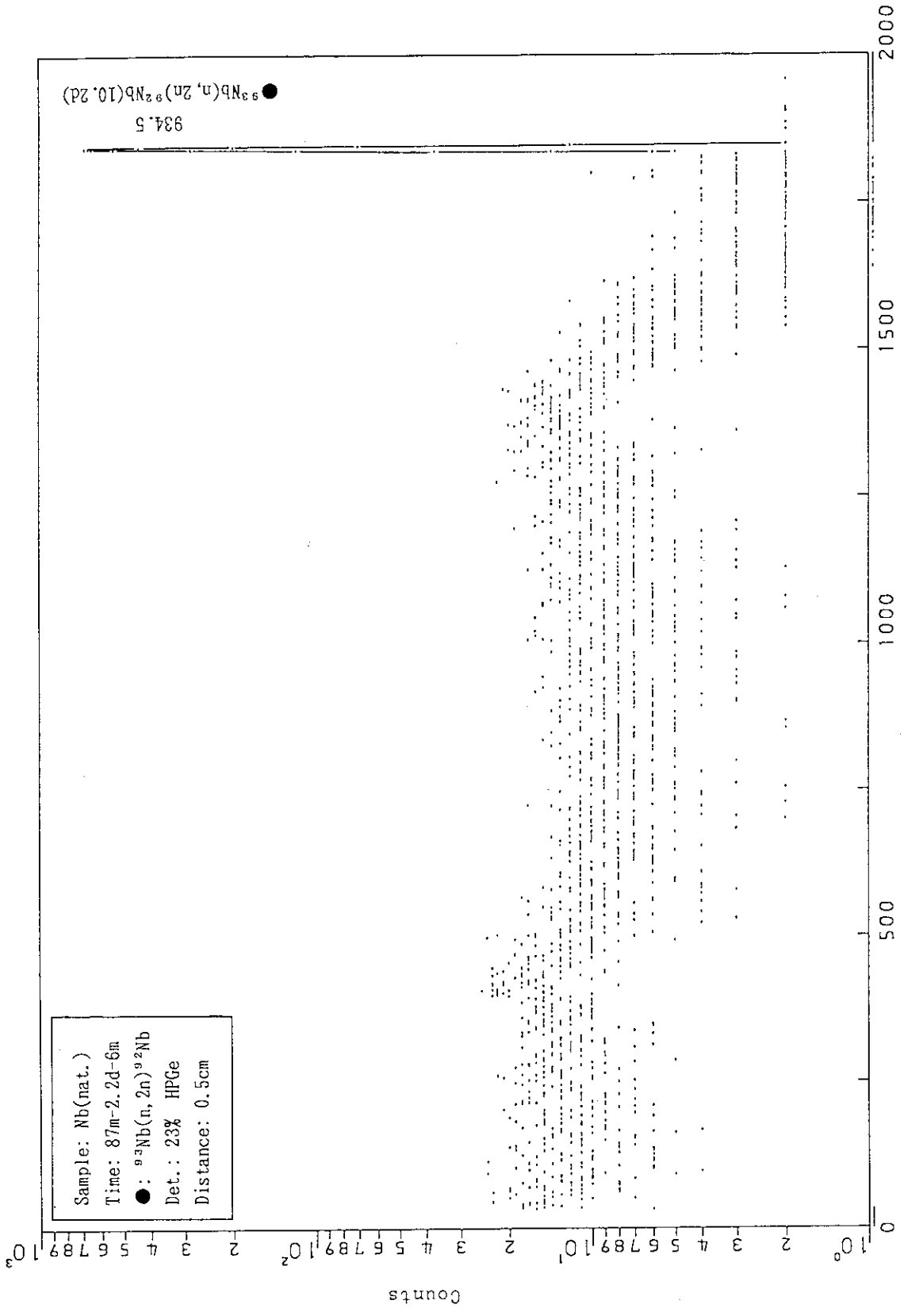
Sample: Nb(nat.)
Time: 87m-2.2d-6m
●: ^{93}Nb(n,2n)^{92}Nb
Det.: 23% HPGe
Distance: 0.5cm
934.5
●^{93}Nb(n,2n)^{92}Nb(10.2d)
Counts
Channel Number
0
500
1000
1500
2000

Fig. A.1.26